1   Reduction in sunlit Earth reflected radiance 317 to 780 nm during the eclipse of 21 August 2017

2   Jay Herman[1], Guoyong Wen[2], Alexander Marshak[3], Karin Blank[3], Liang Huang[4], Alexander Cede[5], Nader

3   Abuhassan[1], Matthew Kowalewski[6]

4   Abstract

5   Ten wavelength channels of calibrated radiance image data from the sunlit Earth are obtained

6   every 65 minutes during Northern Hemisphere summer from the DSCOVR/EPIC instrument located near

7   the Earth-Sun Lagrange-1 point (L_1), 1.5 million km from the Earth. The L_1 location permitted seven

8   observations of the Moon's shadow on the Earth for about 3 hours during the 21 August 2017 eclipse.

9   Two of the observations were timed to coincide with totality over Casper, Wyoming and Columbia,

10   Missouri. Since the solar irradiances within 5 channels (λ_i = 388, 443, 551, 680, and 780 nm) are not

11   strongly absorbed in the atmosphere, they can be used for characterizing eclipse reduction in reflected

12   radiances for the sunlit face of the Earth containing the eclipse shadow. Five channels (λ_i= 317.5, 325,

13   340, 688, and 764 nm) that are partially absorbed in the atmosphere give consistent reductions

14   compared to the non-absorbed channels. This indicates that cloud reflectivities dominate the 317.5 to

15   780 nm radiances reflected back to space from the sunlit Earth's disk with a strong contribution from

16   Rayleigh scattering for the shorter wavelengths. A reduction of 10 % in estimated spectrally integrated

17   radiance (387 to 781 nm) reflected from the sunlit Earth towards L_1 was obtained for two sets of

18   observations on 21 August 2017, while the shadow was in the vicinity of Casper, Wyoming (42.8666° N,

19   106.3131° W, centered on 17:44:50 UTC) and Columbia, Missouri (38.9517° N, 92.3341° W, centered on

20   18:14:50 UTC). In contrast, when non-eclipse days (20 Aug. and 23 Aug.) are compared for each

21   wavelength channel, the change in reflected light is much smaller (less than 1 % for 443 nm compared to

22   9 % (Casper) and 8 % (Columbia) during the eclipse). Also measured was the ratio $R_{EN}(\lambda_i)$ of reflected

23   radiance on adjacent non-eclipse days divided by radiances centered in the eclipse totality region with

24   the same geometry for all 10 wavelength channels. The measured $R_{EN}(443 \text{ nm})$ was smaller for Columbia

25   (169) than for Casper (935), because Columbia had more cloud cover than Casper. $R_{EN}(\lambda_i)$ forms a useful

26   test of 3-D radiative transfer models for an eclipse in the presence of optically thin clouds. Specific

27   values measured at Casper with thin clouds are $R_{EN}(340 \text{ nm}) = 475$, $R_{EN}(388 \text{ nm}) = 3500$, $R_{EN}(443 \text{ nm}) =$

28   935, $R_{EN}(551 \text{ nm}) = 5455$, $R_{EN}(680 \text{ nm}) = 220$, and $R_{EN}(780 \text{ nm}) = 395$. Some of the variability is caused by

29   changing cloud amounts within the moving region of totality during the 2.7 minutes needed to measure

30   all 10 wavelength channels.

32   **Correspondence email: jay.r.herman@nasa.gov**

33   **[1]University of Maryland Baltimore County JCET**

34   **[2]Morgan State University, Baltimore Maryland**

35   **[3]NASA Goddard Space Flight Center, Greenbelt, Maryland**

36   **[4]Science Systems and Applications, Lanham, Maryland**

37   **[5]Goddard Earth Sciences Technology & Research (GESTAR) Columbia, Columbia, MD 21046, USA**

38   **[6]SciGlob Instruments and Services, Elkridge, Maryland USA**

1.0 Introduction

Measured backscattered radiances of the entire sunlit Earth were obtained during the 21 August 2017 eclipse from EPIC (Earth Polychromatic Imaging Camera) on the DSCOVR (Deep Space Climate Observatory) satellite. EPIC obtains synoptic observations of the Earth from an orbit around the L_1 point (Lagrange 1) 1.5 million km from Earth (Herman et al., 2018). EPIC top of the atmosphere TOA albedo measurements, made at a backscatter angle of 172°, are in the enhanced reflectivity regime (hotspot angles). EPIC non-eclipse day TOA albedos are compared to the satellite instrument POLDER (POLarization and Directionality of the Earth's Reflectances) surface reflectivity measurements at 8° (Maignan et al., 2004). This study focuses on data from two selected locations during the 21 August 2017 eclipse that crossed the United States from west to east. The locations selected were Casper, Wyoming and Columbia, Missouri, both near the center of the path of totality and both with a nearly overhead total solar eclipse (local time 11:45 in Casper, Wyoming and 13:12 in Columbia, Missouri). The sites were selected in advance to have a high probability of almost cloud-free skies, and so that totality would occur about 30 minutes apart in UTC (Coordinated Universal Time) to accommodate the satellite's ability to acquire data. On the day of the eclipse, Casper, Wyoming had almost clear skies (Fig. 1), with a small amount of thin clouds visible, while Columbia, Missouri had more low altitude cloud cover (Fig. 2).

Observations of total solar eclipses have been made with varying degrees of sophistication for thousands of years as reviewed by Littman et al. (2008). At a given location, observations of reduced irradiance reaching the Earth's surface are limited to just a few minutes of totality and about two hours of partial obscuration (Meeus, 2003). The totality region (umbra) is an oval of about 110 -120 km in size near local noon at Casper, Wyoming and Columbia, Missouri, but will change size and shape as a function of local solar zenith angle (https://eclipse2017.nasa.gov/eclipse-maps). Some of the complicating factors concerning quantitative eclipse observations include the effects of the solar corona and light scattered in the atmosphere (Liendo, and Chacin, 2004; Emde and Mayer, 2007).

A detailed analysis of an eclipse that occurred in 2006 over southern Europe includes both ground-based and space-based polar orbiting MODIS (Moderate Resolution Imaging Spectroradiometer) observations of cloud cover before totality (Gerasopoulos et al., 2008) as well as theoretical modelling of the eclipse, but unlike the present study, it was largely limited to local effects near the region of totality. A comparison from a meteorological radiation model and measurements of total solar irradiance were made near Athens Greece (84 % of a total eclipse) that showed good agreement in the presence of light clouds (Psiloglou and Kambezidis, 2007). A 3D Monte Carlo radiative transfer study (Emde and Mayer, 2007) was applied to the geometry for the nearly overhead total eclipse of 29 March 2006 (13:20 local time in Turkey) to estimate the downward global radiation at the surface, but without the effect of clouds included in the calculation. An application of the 3D model to the 2006 eclipse over Kastelorizo, Greece with fairly cloud-free measurements (few cumulus, 1-2 octas, and scattered cirrus, 3-4 octas) at 380 nm showed good agreement for the ratio (ratio = 217) of global surface irradiance starting 5 minutes before totality to that during totality (Kazantzidis et al., 2007). Successful modelling of the light levels during an eclipse under realistic conditions is the first step toward improved modelling of high cloud reflection and shadowing of solar radiation on the Earth's energy balance.

79   The observations from the DSCOVR satellite are part of a larger project that combines
80   simultaneously obtained satellite and ground-based measurements using a pyranometer (Ji and Tsay,
81   2000) and the Pandora Spectrometer Instrument (Herman et al., 2009) at both sites. The combination
82   will be used to help validate three dimensional (3D) radiative transfer models applicable to analysis of
83   eclipse effects on radiances reflected back to space and reaching the Earth's surface. This study presents
84   the only calibrated spectral synoptic satellite data of the sunlit Earth ever obtained during an eclipse,
85   which should place tighter limits on validating radiative transfer studies under realistic conditions. The
86   data includes EPIC measured ozone absorption (316±5 DU Casper and 305±5 DU for Columbia, see Fig.
87   A3), O_2 A- and B-band absorption, clouds, aerosols, and scene and surface reflectivity (Herman et al.,
88   2018; Marshak et al., 2018).

89   DSCOVR/EPIC observations of the entire sunlit Earth from the eclipse day, 21 August 2017, are
90   compared to those from two non-eclipse days to quantify the change of the global integral of reflected
91   solar radiation caused by the eclipse. We present a potential validation test data set for the 21 August
92   2017 eclipse for 3D radiative transfer models, namely the ratio of radiances without the eclipse on 20
93   and 23 August to the same regions that contained totality on 21 August 2017 (based on a suggestion in
94   the paper by Emde and Mayer, 2007).
95
96   Section 2 describes the DSCOVR/EPIC instrument, available data, and monochromatic images based
97   on measured counts per second, C/s. Section 3.1 presents a comparison between eclipse and non-
98   eclipse days. Section 3.2 gives an estimate of the global reduction of reflected sunlight during the eclipse
99   over Casper, WY and Columbia, MO.
100

101   **2.0 EPIC Instrument and Data Description**

102   The EPIC instrument onboard the DSCOVR spacecraft, in a six-month orbit near the L_1 point
103   since June 2015, observed the Moon's shadow for about 3 hours. The EPIC data comprises a set of seven
104   observations (16:44 to 19:44 UTC) starting in the Pacific Ocean and ending in the Atlantic Ocean, while
105   synoptically observing the entire sunlit disk of the Earth (nominal size 0.5^O). EPIC is a 10 wavelength
106   filter camera with a 2048x2048 pixel CCD (charge couple detector) using a 30-cm aperture Cassegrain
107   telescope with a field of view (FOV) of 0.62^O that continuously points at the sunlit Earth. The sampling
108   size on the Earth is nominally 8 km at the center of the image with an effective spatial resolution of
109   10x10 km^2 for the 443 nm channel and 17x17 km^2 for the other 9 filter channels. Operation of EPIC
110   consists of sequentially selecting a filter from 2 rotatable filter wheels and an exposure time using a
111   rotating disk shutter mechanism. Invariant exposure times were set at the beginning of the on-orbit
112   mission to fill the CCD wells to about 80 % and avoid blooming (a saturated pixel affecting its neighbors).
113   The CCD was calibrated for the sensitivity differences between the pixels (flatfielding), and
114   measurements were made in the laboratory and in-flight to obtain corrections for stray light effects.
115   Corrections for dark current are applied based on periodic measurements with the shutter closed. EPIC
116   is kept centered on the Earth during its 6-month north-south tilted Lissajous orbit about the Earth-Sun L_1
117   point. The spacecraft is never closer than 4° from the Earth-Sun line, which makes it possible to observe

118   an eclipse without the Moon being in the FOV. On 21 August 2017, DSCOVR was 7.7^O from the Earth-Sun
119   line. A more detailed description of EPIC is given in Herman et al. (2018) and Marshak et al., (2018).

120   The geolocated EPIC data (Counts per second, C/s) from each set of 10 wavelengths are
121   contained in an HDF5 formatted file available from the permanent NASA Langley data repository center
122   (https://eosweb.larc.nasa.gov/project/dscovr/dscovr_epic_l1b). Contained in each Level-2 data HDF5 file
123   are the 2048 x 2048 array of C/s measured by EPIC and a common latitude and longitude grid. The
124   geolocated data are organized corresponding to the rectangular CCD grid, 1 data point per CCD pixel.
125   For the time of the eclipse, the illuminated CCD pixels are within a circular boundary corresponding to
126   Np = 2.59x10^6 illuminated pixels (illuminated pixels formed a circle of 1816 pixels in diameter out of a
127   maximum of 2048 pixels. To reduce the volume of telemetry data, all measurements, except those from
128   the 443 nm channel, were 2x2 averaged onboard DSCOVR to 1024 x 1024 pixels. After geolocation onto
129   a common latitude x longitude grid, the data from all channels are presented as 2048 x 2048 points with
130   off-earth points represented as the floating point symbol for "infinity". All of the data products (e.g.,
131   ozone amounts) are also freely available at the above repository center.

132   The EPIC HDF5 file names (e.g., epic_1b_20170821174450_02.h5) from the NASA data
133   repository are interpreted as Year 2017, Month 08, Day 21, UTC 17:44:50, Version 2, which is 11:44:50
134   local daylight savings time in Casper, Wyoming. The filename time refers to approximately the middle of
135   the measurement sequence. Totality in Casper started at 11:42:39 and ended at 11:45:05. Version 2
136   refers to the reprocessing of data with the latest CCD flat-fielding and stray-light corrections (Herman et
137   al., 2018; Marshak et al., 2018; Geogdzhayev and Marshak, 2017), and the geolocation algorithms.

138   The observing conditions for 21 August 2017 ranged from significant cloud cover over the oceans to
139   nearly clear skies over the United States (Figs. 1 and 2). The synoptic observations provided a unique
140   opportunity to estimate the fraction of reduced reflected radiation from the entire sunlit Earth caused
141   by a total solar eclipse. Two of the synoptic observations were timed so that they centered on Casper,
142   Wyoming (42.8666° N, 106.3131° W, 17:44:50 UTC) and Columbia, Missouri (38.9517° N, 92.3341° W,
143   18:14:50 UTC). Ten narrowband images were obtained at center vacuum wavelengths λ_i of 317.5±0.5,
144   325±0.5, 340±1.3, 388±1.3, 443±1.3, 551±1.5, 680±0.8, 688±0.42, 764±0.5 and 779.5±0.9 nm (Herman
145   et al., 2018). Of these, 388, 443, 552, 680, and 779 nm radiances are not strongly absorbed in the
146   atmosphere and are used for estimating the reduction in reflected radiances from the Earth. The others
147   are strongly affected either by ozone (317, 325, 340 nm) or oxygen absorption (688, 764 nm) in the
148   atmosphere, but give similar radiance percent reductions during the eclipse compared to non-absorbed
149   channels.

150   The non-absorbed wavelength observations were combined to produce eye-realistic color images
151   (https://epic.gsfc.nasa.gov). For this eclipse day study, 21 August, the original color images were
152   modified by increasing the gamma correction to better show the umbra over Casper, Wyoming and
153   Columbia, Missouri (Figs. 1 and 2 based on a suggestion by Steven Albers and Michael Boccara, 2017,
154   Private Communication). The images include Rayleigh scattering effects that cause light from the
155   penumbral region to increase illumination within the umbra along with scattering from clouds and
156   aerosols.

4

157   Table 1 summarizes eclipse timing and location details for Casper, Wyoming. During the 2.7
158   minutes needed to obtain all 10 wavelength channel images, the center of totality moves at about 46
159   km/minute or covering approximately 124 km. Based on the image in Fig. 1, the entire measurement
160   took place within the observed nearly clear-sky region surrounding Casper, Wyoming. A similar table
161   could be constructed for the eclipse totality region near Columbia, Missouri.

Table 1 *Eclipse Measurement Timing and Location Details for 5 Wavelengths*
Eclipse Maximum and EPIC Image Times. Total Measurement Duration 2.7 minutes

Wavelength (nm)	Date and Time	Location Name	Longitude
	2017-08-21 17:35:40	Eclipse West Edge of WY state	$-111^{\circ}02'$
551	2017-08-21 17:42:36	West of Casper	$-106^{\circ}22'$
680	2017-08-21 17:43:30	West of Casper	$-106^{\circ}21'$
Casper Wyoming	2017-08-21 17:43:51	Casper WY	$-106^{\circ}19'$
780	2017-08-21 17:44:24	Near Glenrock WY	$-105^{\circ}52'$
443	2017-08-21 17:44:50	West of Douglas WY	$-105^{\circ}14'$
388	2017-08-21 17:45:18	West of Douglas WY	$-105^{\circ}17'$
	2017-08-21 17:48:04	Eclipse East Edge of WY state	$-104^{\circ}03'$

162

163   The timing and predicted shape of the Moon's shadow over Casper, Wyoming and Columbia,
164   Missouri can be seen at https://eclipse2017.nasa.gov/eclipse-maps. An annotated portion of the figures
165   for Casper and Columbia are reproduced in the Appendix (Fig. A1). The predicted totality shadow (Fig.
166   A1) over Casper was elliptical in shape with a width of about 116 km (about 1.5° in latitude or
167   longitude). The similar drawing for Columbia, Missouri shows a more nearly circular region of totality.
168   The dimension of the partial eclipse for 90 % obscuration is about 5° in latitude or longitude. The region
169   of 75 % obscuration covers a latitude range 32° to 46° or about 1200 km. An obscuration region of this
170   size produces a significant decrease in the percentage of total solar irradiance reaching the Earth's
171   surface and in the amount reflected back to space. EPIC synoptically measures both the local and sunlit
172   portion of the global percent change in reflected radiance, which is approximately the same as the
173   percent change in global surface irradiance for the wavelength range from 388 to 780 nm. An exception
174   is within the umbral region, where the percent change is larger at the surface than at the top of the
175   atmosphere. The three wavelength channels shorter than 388 nm are affected by ozone absorption and
176   also do not contribute much to the sum of reflected radiances compared to the range from 388 to 780
177   nm. The energy content of 317 to 340 nm are not included in the quantitative estimate of broadband
178   (UV + visible) reduced reflected radiance, nor are the strongly absorbed O_2 A- and B-band channels, 688
179   and 764 nm, included. However, the effects of the eclipse on all 10 channels are individually estimated.
180

181   **2.1 Monochromatic Eclipse Images**

182

183   Before quantitatively examining the EPIC data from the eclipse in units of C/s or reflectance, the
184   same data can be represented as monochrome grey-scale images. The images (Fig. 3 with North down)
185   range from 340 nm, with strong Rayleigh scattering effects and some ozone absorption, to 780 nm in
186   the near infrared. North is selected as down to correspond to a 3D projection image presented later.

187 Because of the clarity of the atmosphere at 780 nm, the image serves as a geographic map of the Earth
188 as viewed by EPIC where North and South America are clearly visible.
189
190 **3.0 Results**

191 **3.1 Comparison of EPIC Observations of Eclipse Totality (21 Aug) with Non-Eclipse Days (20 and 23**
192 **Aug) for Casper, WY and Columbia, MO**

193   Atmospheric conditions during the eclipse at Casper, Wyoming were almost cloud-free
194 compared to Columbia, Missouri, which had optically thin low altitude clouds (Fig. 2). Figure 4 shows the
195 cloud cover on the day of the eclipse, 21 August 2017 (panel A) about 90 minutes before totality at
196 Casper and about 2 hours after totality. The eclipse umbra is still visible over the Atlantic Ocean. The
197 images (north is up) show that the skies remained relatively clear over the northern United States for
198 the duration of the eclipse. A similar set of images (panel B) are shown for the day before (20 August)
199 and two days after the eclipse (23 August). There was no useable data available on 22 August. Data
200 obtained on 20 and 23 Aug. at approximately the same UTC (backscatter phase angle for a given location
201 on Earth) as occurred during the total eclipse are used as reference data to compare with the eclipse
202 data on 21 Aug. The basic global patterns of cloud cover are similar for all three days, but not identical.
203 As shown later, the amount of light reflected back to space is approximately the same on the two non-
204 eclipse days 20 August and 23 August.

205   Figure 5 (upper panels A and B) shows longitudinal slices of 443 nm reflected solar radiances in
206 C/s towards L_1 through the locations corresponding to Casper, Wyoming and Columbia, Missouri at their
207 respective times of totality. The lower panels (C and D) of Fig. 5 show 443 nm measurements in C/s on
208 20 Aug at 18:04 UTC before the eclipse for nearly identical solar phase angles conditions for both sites.
209 The effect of clouds at the Columbia site compared to Casper can be seen in terms of the depth of the
210 umbra relative to the average C/s from -140° to -150° longitude (Panels A: ratio = 1530 and B: ratio =
211 37). Similarly, on the preceding day, 20 Aug (panels C and D), the cloud effect is small at Casper, 1.2×10^4
212 C/s, compared to Columbia, 5×10^4 C/s and just to the west of Columbia, 1.3×10^5 C/s.
213
214   The minimum 443 nm values during totality are 16.6 C/s for Casper and 312 C/s for Columbia.
215 On 20 Aug. EPIC measured 15240 C/s and 52728 C/s, respectively, showing the effect of increased
216 cloudiness for Columbia. While Fig. 5 is expressed in C/s, the data can be converted to radiance W/(m^2
217 nm sr) based on an in-flight determined radiance calibration coefficient of K_R(443nm) = 5.291×10^{-6}
218 W/(m^2 nm sr C/s) derived from reflectance coefficients (Geogdzhayev and Marshak, 2017; Marshak et
219 al., 2018; Herman et al. 2018). For 443 nm channel, an average count rate for the illuminated earth is
220 3×10^4 C/s corresponding to a radiance of 0.159 W/(m^2 nm sr). EPIC calibration constants for 8 of the 10
221 channels were obtained by in-flight comparisons of reflectance measured by two well calibrated low
222 Earth orbiting satellite instruments, OMPS (Ozone Mapping Profiler Suite for UV channels) and MODIS
223 (Moderate Resolution Imaging Spectroradiometer for visible and near-IR channels) for simultaneously
224 viewed Earth areas with the same satellite view and solar zenith angles (Herman et al., 2018;
225 Geogdzhayev and Marshak, 2017). The O_2 A- and B-band channels were calibrated using lunar data
226 when the Moon was within the field of view of EPIC. Detailed discussions and values of all EPIC

227 calibration coefficients K(λ) are given by Geogdzhayev and Marshak (2017), Herman et al, (2018) and
228 Marshak et al., (2018). Most of the conclusions in this study are in terms of ratios of C/s from the same
229 wavelength channel at approximately the same solar phase angle that are independent of the absolute
230 calibration conversion from C/s to radiance.
231
232   The ratio $R_{EN}(\lambda_i)$ = I(20 August)/I(21 August) is used to characterize the eclipse effects at the top
233 of the atmosphere. Because the solar phase angles are nearly the same, the effects of the 172°
234 backscatter angle ("hot spot" caused mostly by minimized shadows) and ocean specular reflection are
235 also nearly the same on both days.

236   There is considerable variability in $R_{EN}(\lambda_i)$ as a function of wavelength that is partially caused by
237 the 2.7 minutes needed to obtain measurements for all 10 wavelengths. During the 2.7 minutes, the
238 center of totality moved about 124 km or about 1.7^O longitude, meaning that the ratio was affected by
239 atmospheric variability (mostly cloud effects) in the successive scenes containing the eclipse totality for
240 each wavelength. The ratios $R_{EN}(\lambda_i)$ of C/s on the eclipse day to the preceding non-eclipse day are shown
241 in Fig. 6 for all 10 wavelength λ_i channels and two sites (Casper, Fig 6a and Columbia, Fig. 6b) and
242 summarized in Table 2. The same reference data from 20 Aug is used for both sites, since it was the
243 closest in UTC for both the Casper and Columbia eclipse times.

244

245 *Table 2 Maximum Radiance Ratio $R_{EN}(\lambda_i)$ during eclipse totality 17:44:50*
246 *UTC (Casper) and   18:14:50 UTC (Columbia) compared to 20 Aug. at*
18:03:59 for both sites (see Fig. 6).

Wavelength λ_i (nm)	Max. $R_{EN}(\lambda_i)$ C/s Casper, Wyoming	Max. $R_{EN}(\lambda_i)$ C/s Columbia, Missouri
317.5	255	50
325	245	49
340	475	59
388	3500	81
443	935	169
551	5455	183
680	220	171
688	365	246
764	302	92
780	395	38

247   For the eclipse study, the range of synoptically observed longitudes is approximately from the
248   international dateline (-180°) to almost longitude of Greenwich, England (0°). The nearly clear-sky in
249   Casper with optically thin clouds permits the reflected light during totality to become very small (about
250   17 C/s for 443 nm compared to 1.5x10^4 C/s on 20 August at the same longitude). Columbia had more
251   low altitude cloud cover than Casper (Fig. 2) with the cloud cover extending into the region of totality.
252   The effect of this cloud cover can be seen in Fig. 6, where the maximum R_{EN}(443, Columbia) = 169
253   compared to 935 for Casper. Table 2 provides the eclipse radiance ratio $R_{EN}(\lambda_i)$ for the five non-absorbed
254   wavelength and 5-absorbed channels that can help validate 3D radiative transfer models. The measured
255   lower values $R_{EN}(\lambda_i)$ at Columbia compared to Casper show that there is high sensitivity in the TOA
256   upwelling measured ratios to the presence of even optically thin clouds. A detailed radiative transfer
257   study for realistic conditions is made feasible by using EPIC's simultaneous estimates of cloud reflectivity
258   and transmission, cloud height, ozone amounts, (Fig. A3 and Herman et al., 2018), and aerosol amounts
259   (Torres et al., 2018 private communication). These data products are available from the NASA-Langley
260   data repository referenced above.

261
262   **3.2 Global reduction of reflected sunlight during the eclipse over Casper WY**
263
264   The unique DSCOVR/EPIC measurements provide estimates of the fractional reduction of
265   sunlight from 388 to 780 nm reflected back to space for the entire sunlit globe caused by the eclipse
266   shadow on the Earth. To do this, all of the light reaching EPIC in each of the five non-absorbed channels,
267   388, 443, 551, 680, and 780 nm, are integrated over the visible sunlit Earth and compared (percent
268   difference PDF(λ_i)) with a nearly identical viewing geometry (nearly the same UTC) from the previous
269   and next days. The assumption is that the major cloud features change slowly on a global scale over
270   relatively short periods (Figs. 1 to 3). A test of this hypothesis is that the PDF between successive non-
271   eclipse days is small compared to the eclipse day PDF(λ_i) with a non-eclipse day.

272   In the 3D Fig. 7 for 443 nm, the nearly cloud free eclipse region is the blue area in the midst of
273   greens, yellows, and reds. The high red values correspond to fairly reflective clouds mostly seen near
274   the equator (Fig. 1). The yellows and greens correspond to lower altitude clouds that tend to have
275   smaller reflectivities. Integrating over all of the pixels for the eclipse on 21 August 2017, using the file
276   named epic_1b_20170821174450_02.h5, we get S(DOY, UTC) = 5.34366x10^{10} C/s for DOY=233 (21
277   August 2017) and UTC=17:44:50. For the eclipse day, the 443 nm average C/s = 2.0631x10^4, which
278   corresponds to 2.0631x10^4 K_R(443 nm) = 0.11 W/(m^2 nm sr). Peak values are approximately 1x10^5 C/s,
279   or about 0.53 W/(m^2 nm sr). Figure 7 is oriented with north down so as to be able to see into the eclipse
280   shadow region. A similar figure is obtained for Columbia, Missouri with reduced depth caused by some
281   visible light cloud cover extending into the region of totality (Fig. 2).

282

283   Measured C/s images for six wavelength channels (340 to 780 nm) on 20, 21, and 23 August (Fig.
284   8) were selected to be as close as possible to the UTC time of the eclipse in Casper Wyoming, keeping
285   the scattering phase angles nearly constant. Similar images for the strongly absorbed channels 317.5,

8

286   325, 688, 764 nm channels are shown in the appendix (Fig. A2). The middle images in panels B and E of
287   Figs. 8a, 8b and 8c are for the eclipse over Casper, Wyoming. These images are in the same format as
288   Fig. 3, but rotated with north up. Unlike Fig. 3, the scale in Fig. 8 was selected so that the brightest
289   clouds do not saturate the image. The increase in scale makes the land surfaces less visible. While the
290   figures are similar from wavelength to wavelength, there are differences in the depth of the eclipse
291   totality and the reflectivities of the surrounding clouds. In general, the equatorial clouds with higher C/s
292   (reflectivities) tend to reach higher altitudes. This is confirmed by examining the C/s in the strongly
293   absorbed O_2 A-band channel (Fig. A2b and Herman et al., 2018).

294   EPIC measured $C(\lambda)$ in C/s for each pixel can be converted to Earth top of the atmosphere
295   reflectance $Re(\lambda)$ using the in-flight derived calibration coefficients $K(\lambda)$, where $Re(\lambda) = K(\lambda) C(\lambda)$. For
296   the six wavelength channels in Fig. 8 plus the O_2 A- and B-band channels, $K(340) = 1.975 \times 10^{-05}$, $K(388) =$
297   2.685×10^{-05}, $K(443) = 8.340 \times 10^{-06}$, $K(551) = 6.66 \times 10^{-06}$, $K(680) = 9.30 \times 10^{-06}$, $K(687.75) = 2.02 \times 10^{-05}$, $K(764)$
298    $= 2.36 \times 10^{-05}$, and $K(780) = 1.435 \times 10^{-05}$ (Herman et al., 2018; Geogdzhayev and Marshak, 2018; Marshak
299   et al., 2018). To estimate the percent reduction in outgoing radiances, the ratios of integrals over the
300   illuminated CCD for each wavelength channel are formed for nearly the same Earth geometry on days
301   preceding and following the eclipse. Either the integrated reflectances or the integrated C/s x 10^{-7} (Eqn.
302   1) for Tables 3A for Casper, Wyoming and 3B for Columbia Missouri) over the CCD pixels, $ICs(\lambda)$, can be
303   used directly, since they are linearly proportional to the integral of the photons received by the
304   illuminated pixels.

305

306   Table 3 and Fig. 9 show that the global reduction of backscattered light caused by the eclipse is
307   similar for the two sites even though there is more cloud cover locally over Columbia than Casper. This is
308   because the global reduction caused by the differing umbral regions is a small fraction of the total, and
309   only 30 minutes have elapsed between the two measurements, which is not enough time for the global
310   cloud cover to have significantly changed.

311

Table 3A Global integral of reflected light ICs for the UTC of the Casper, WY eclipse on 21 August and for the closest solar phase angle from 20 and 23 August. PDF is the percent difference caused by the eclipse. Units are ICs x 10^{-7}

λ_i (nm)	20 August 2017 16:58:31 UTC	21 August 2017 17:44:50	23 August 2017 17:54:36	Avg. PDF
317.5	280.5	258.8	282.0	9±0.3
325	460.6	425.5	464.2	9±0.4
340	3183	2946	3213	9±0.5
388	2034	1878	2044	9±0.3
443	5808	5344	5813.2	9±0.05
551	5619	5078	5573	10±0.5
680	3790	3433	3773	10±0.3
688	1129	1010	1110	11±0.9
764	671.9	585.9	651.9	13±1.7
780	2794	2491	2799	12±0.1

312

Table 3B Global integral of reflected light ICs for the UTC of the Columbia, MO eclipse on 21 August and for the closest solar phase angle from 20 and 23 August. PDF is the percent difference caused by the eclipse. Units are ICs x 10^{-7}

λ_i (nm)	20 August 2017 18:03:359 GMT	21 August 2017 18:14:50	23 August 2017 17:54:36	Avg. PDF
317.5	281.3	258.3	282.0	9±0.1
325	461.6	425.9	464.2	9±0.3
340	3193	2956	3213	8±0.3
388	2034	1884	2044	8±0.3
443	5813.7	5372.3	5813.2	8±0.01
551	5586	5091	5573	10±0.1
680	3790	3453	3773	10±0.2
688	1121	1011	1110	10±0.5
764	661.2	576.0	651.9	14±0.8
780	2794	2475	2799	13±0.1

313 Figure 9 shows a plot of the data contained in Table 3 based on Eqn. 1. The two non-eclipse days are
314 nearly identical, while the eclipse day (21 Aug) is significantly lower at all wavelengths. The
315 backscattered light (in C/s) peaks near 500 nm and then decreases toward longer wavelengths, since
316 C(λ) is proportional to the solar irradiance, which decreases with λ after approximately 550 nm.

$$ICs(\lambda) = \int_{0}^{2048} \int_{0}^{2048} C(\lambda, x, y)dxdy \tag{1}$$

over Np = 2.59x10^6 illuminated pixels on 20, 21, 23 August 2017

317

318

319   For the 443 nm channel, the result is an approximate decrease of 9 % on 21 August at 11:44:50
320 for Casper and 8% at 12:14:50 for Columbia local time. As a reference, we compare two non-eclipse
321 days (20 and 23 August). The relative difference is (5808-5813)/5813 0.1 % for Casper and 0.01 % for
322 Columbia, which is much smaller than the 9 % decrease produced by the eclipse on 21 August. The
323 comparison of the 443 nm eclipse day with two non-eclipse days gives a measure of the uncertainty in
324 the calculation (e.g., 9 ± 0.05 % for Casper and 8 ± 0.01% for Columbia).

325

326   Percent difference PDF(λ_i) calculations for λ_i = 317.5, 325, 340, 388, 443, 551, 680, 688, 764, and
327 780 nm, based on Eqn. 1 are summarized in Table 3A, yielding PDF(λ_i) = 9, 9, 9, 9, 9, 9, 10, 10, 13, and 12
328 % reductions in backscattered radiances in the direction of L$_1$, respectively for Casper with similar values
329 for Columbia. The PDF(764 nm) within the strongly absorbing O$_2$ A-band is 13 % for Casper and 14% for
330 Columbia, even though the reflected ICs(764nm) is much lower than the surrounding non-absorbed
331 bands. The fact that adjacent absorbed and non-absorbed wavelengths give consistent PDF(λ_i) suggests
332 that most of the effect comes from clouds. Eclipse effects for the short UV wavelengths are affected by
333 Rayleigh scattering and clouds, and not much by the relatively low UV surface reflectivity (about 4%).
334 Eclipse effects on outgoing radiances for wavelengths longer than about 700 nm are increased by
335 vegetation reflectivity, even where the amount of clear-sky penetrating radiances are small for the O2

336

338

339   To estimate the fractional reflected radiance reduction for the wavelength range from 388 to
340 780 nm, a polynomial interpolation $R(\lambda)$ of the Avg. PDF in Table 3 for the 5 weakly absorbed channels is
341 formed (Fig. 10 panels A and B red curves). $R(\lambda)$ must be weighted by the solar irradiance spectrum $F(\lambda)$.
342 The solar spectrum used is a combination of measured solar flux data named "atlas_plus_modtran" in
343 the libRadtran software package (Mayer and Kylling, 2005). The components, F_R and F_S, of the weighted
344 average R are defined in Eqns. 2 and 3. On 21 August 2017 the distance of the Earth from the Sun was
345 1.011 AU, or F_S(21 Aug at 1 AU) = 664.94 W/m^2 and at 1 AU, $F_{R-Casper}$ = 66.11 W/m^2 and $F_{R-Columbia}$ = 64.86
346 W/m^2. For the wavelength range of interest (387.9 to 781.25 nm), F_S is about half of the total solar
347 irradiance of 1361 W/m^2 at the top of the atmosphere at 1 AU (Kopp and Lean, 2011).

348

349

$$F_S = \int_{387}^{781} F(\lambda)d\lambda \qquad\qquad F_R = \int_{387}^{781} R(\lambda)F(\lambda)d\lambda \qquad (2)$$

$$< R >= \frac{\int_{387}^{781} R(\lambda)F(\lambda)d\lambda}{\int_{387}^{781} F(\lambda)d\lambda} \qquad\qquad \begin{aligned} &<R_{Casper}> \ = 0.101 \\ \\ &<R_{Columbia}> = 0.098 \end{aligned} \qquad (3)$$

350   Figure 11b shows the product $R(\lambda)F(\lambda)$ /F_S (nm^{-1}). Forming <R> shows that during the eclipse the
351 shadow of the Moon reduces the backscattered radiance (388 to 780 nm) from the sunlit Earth in the
352 direction of L_1 by about 10 %. The combined uncertainty ±0.3 % is caused by variations in the cloud
353 cover of the reference days compared the eclipse day. The calculation of <R> is based on C/s
354 measurements from DSCOVR/EPIC of the sunlit Earth and the interpolation function $R(\lambda)$. The result is
355 independent of the absolute calibration of EPIC, since it is based on ratios of C/s over three days with
356 approximately the same UTC (scattering phase angles). $R(\lambda)$ includes the near backscatter direction
357 enhanced reflection function appropriate for the entire sunlit disk at a backscatter angle of about 172°.
358 The three days at nearly the same UTC can be compared directly, since EPIC has proven to be very stable
359 based on repeated in-flight calibrations over a 2-year period using OMPS and MODIS (Herman et al.,
360 2018 and Geogdzhayev and Marshak, 2018). The smooth function $R(\lambda)$ does not include absorption
361 features from water and the O_2 A- and B-bands.

362

3.3 Comparison of EPIC albedo with POLDER reflectance

The TOA albedo measurements made by EPIC can be compared with reflectance measurements made by the POLDER satellite instrument near the hotspot backscatter direction (172°) for the incident solar irradiance over nearly cloud-free scenes (Maignan et al., 2004). EPIC C/s can be converted to albedo using the calibration constants K(λ), which already contains the factor π (Fig. 11A). The average TOA albedo from EPIC was almost the same on 20 Aug. as on 23 Aug. For EPIC albedo data over grassland common to Casper, Wyoming compared to the POLDER measurements, the C/s data for each wavelength (see Fig.5 for 443 nm) can be converted to TOA albedo.

Measurements from the POLDER satellite over Khingan Range, China (117.55°E to131.56°E, 45.68°N to 53.56°N) show that the backscatter amount from the land surface increases with increasing wavelength (Maignan et al., 2004). The Khingan range is mainly covered by deciduous broadleaf and a mix of deciduous and evergreen needle leaf forest with a small amount of grassland, while the area around Casper is mainly short grass prairie land with few trees. Over Casper, WY (Fig. 11B), the wavelength dependence of the EPIC TOA albedo (551, 680, and 780 nm) at 172° backscatter angle is similar to POLDER surface reflectance at 8°. The shape and magnitude differences are partially caused by the atmospheric component of the albedo that includes some light cloud cover, whereas the POLDER reflectance has atmospheric effects subtracted. The effect of increasing Rayleigh scattering is seen for shorter wavelengths measured by EPIC.

3.0 Summary

The EPIC instrument onboard the DSCOVR spacecraft synoptically observes the entire sunlit portion of the Earth from an orbit near the Earth-Sun Lagrange-1 point. On 21 August 2017, EPIC was able to observe the totality shadow from the lunar eclipse of the Sun with the Earth's surface for about 3 hours (seven 10-channel measurements) as it crossed the United States from west to east (about 1.5 hours). When the region of totality was over Casper, Wyoming at 17:44:50 UTC, the reflected 443 nm TOA radiance was reduced to 16 C/s ($8x10^{-5}$ W/m^{2}sr) in the narrow region of totality compared to a non-eclipse day ($1.52x10^4$ C/s or 0.076 W/m^{2}sr). About 30 minutes later the shadow passed over Columbia, Missouri, but the presence of thin clouds in the vicinity of Columbia caused increased reflected radiance of 312 C/s ($1.6x10^{-3}$ W/m^{2}sr) into the umbral region during totality compared to Casper. The ratio $R_{EN}(\lambda_i)$ of reflected radiances within the eclipse totality to radiances for the same geometry on adjacent non-eclipse days was measured for all 10 wavelength channels. The measured R_{EN}(443 nm) was smaller for Columbia (71) than for Casper (936), showing the sensitivity to increased cloud cover over Columbia. Similarly R_{EN}(388 nm, Casper) = 3500 and R_{EN}(388 nm, Columbia) = 81. While the results cannot be directly compared with R_{EN}, good agreement was obtained (Kazantzidis et al., 2007) between a model study based on a 3D Monte Carlo radiative transfer model (Emde and Mayer, 2007) and measured ratio at 380 nm (ratio = 217) of downward global surface radiation before and during totality. The measured radiance ratios $R_{EN}(\lambda_i)$ can serve as a validation data set for 3D radiative transfer models of the atmosphere that include cloud effects, since EPIC also measures the surrounding amount of cloud cover for the entire sunlit Earth. Comparing $R_{EN}(\lambda$, Casper) with $R_{EN}(\lambda$, Columbia) shows that Rayleigh

403 scattering combined with low optical depth clouds can scatter light into the umbra region and reduce
404 $R_{EN}(\lambda)$. Outside of the region of totality, EPIC observed the partial eclipse shadow and the fully
405 illuminated regions of the Earth's disk. Interpolating in wavelength between the percent reductions in
406 integrated radiances (in C/s) over the sunlit globe, $ICs(\lambda_i)$ for the 5 measured non-absorbed wavelength
407 channels at both locations showed that the integrated reflected radiance from the Earth's sunlit disk
408 towards L_1 decreased by about 10 % compared to the integrated radiances measured on the days before
409 and after the eclipse for approximately the same observing geometry as occurred during the eclipse.
410 Similar calculations comparing two non-eclipse days show smaller changes in ICs (less than 0.1 %) than
411 the eclipse-day change. The five channels that are partially absorbed in the atmosphere give consistent
412 results compared to the non-absorbed channels suggesting that cloud reflectivities dominate the 317.5
413 to 780 nm radiances reflected back to space from the sunlit Earth's disk with a contribution from
414 Rayleigh scattering for the shorter wavelengths.

415

Appendix

The course of the eclipse in the vicinity of Casper, Wyoming and Columbia, Missouri is shown in Fig. A1

Greyscale images for the short UV wavelength channels (317.5, 325) with strong ozone absorption and Rayleigh scattering, the longer wavelength UV channels (340, 388), and the strongly absorbed O_2 B- and A-band channels (688, 764 nm) are shown in Figs. A2a, A2b, A2c

The amount of ozone over the eclipse sites can be derived (Herman et al., 2018) to produce ozone data that is stored in the NASA-Langley archive. During the eclipse, it is not possible to derive the amount of ozone from either ground-based or satellite data. Ozone amounts do not change rapidly from day to day except when major weather systems pass through a region, which was not the case during the eclipse period, 20 August to 23 August. This is confirmed from OMI satellite data (Ozone Monitoring Instrument onboard the AURA satellite). Figure A3 shows the amount of ozone over the eclipse trajectory obtained on 20 August. The values obtained 316 DU near Casper, WY and 306 DU near Columbia compare well with ozone amounts derived from OMI of 314 DU and 301 DU. The O_3 variability during the 2.7 minutes (approximately 124 km or about 1^O of longitude) is about ±5 DU.

4.0 Author Contributions

Jay Herman wrote most of the paper and performed most of the calculations

Guoyong Wen is the funded principal investigator of the project.

Alexander Marshak provided the calibration coefficients for the visible and near-IR channels

Karin Blank provided the color images in Figs. 1 to 3. She was responsible for the geolocation of the 10 filter images on a common grid.

Liang Huang provided the calibration coefficients for the UV channels

Alexander Cede provided the flatfielding, stray light correction, and dark current analysis

Nader Abuhassan helped with flatfielding and stray light correction and was responsible for the ground-based portion of this research.

Matthew Kowalewski provided the flatfielding, stray light correction, and dark current analysis

The authors declare that they have no conflict of interest.

5.0 References

Cescatti, Alessandro, Indirect estimates of canopy gap fraction based on the linear conversion of hemispherical photographs: Methodology and comparison with standard thresholding techniques, Agricultural and Forest Meteorology, 143, 1-12, 2007.

Cleveland, William S., LOWESS: A program for smoothing scatterplots by robust locally weighted regression. The American Statistician. **35** (1): 54. JSTOR 2683591. doi:10.2307/2683591, 1981.

Emde, C. and B. Mayer, Simulation of solar radiation during a total eclipse: a challenge for radiative transfer,(2007) Atmos. Chem. Phys., 7, 2259–2270, 2007.

Geogdzhayev, I. V. and Marshak, A.: Calibration of the DSCOVR EPIC visible and NIR channels using MODIS Terra and Aqua data and EPIC lunar observations, Atmos. Meas. Tech., 11, 359-368, https://doi.org/10.5194/amt-11-359-2018, 2018.

Gerasopoulos, E., Zerefos, C. S., Tsagouri, I., Founda, D., Amiridis, V., Bais, A. F., Belehaki, A., Christou, N., Economou, G., Kanakidou, M., Karamanos, A., Petrakis, M., and Zanis, P.: The total solar eclipse of March 2006: overview, Atmos. Chem. Phys., 8, 5205-5220, https://doi.org/10.5194/acp-8-5205-2008, 2008.

Herman, J.R., Alexander Cede, Elena Spinei, George Mount, Maria Tzortziou, Nader Abuhassan, (2009) NO_2 Column Amounts from Ground-based Pandora and MFDOAS Spectrometers using the Direct-Sun DOAS Technique: Intercomparisons and Application to OMI Validation, J. Geophys. Res., 114, D13307, doi:10.1029/2009JD011848, 2009.

Herman, J.R., R.D. Evans, A. Cede, N.K. Abuhassan, I. Petropavlovskikh, and G. McConville, (2015) Comparison of Ozone Retrievals from the Pandora Spectrometer System and Dobson Spectrophotometer in Boulder Colorado, Atmos. Meas. Tech., 8, 3407–3418, 2015 doi:10.5194/amt-8-3407-2015

Herman, Jay, Liang Huang, Richard McPeters, Jerry Ziemke, Alexander Cede, and Karin Blank, Synoptic ozone, cloud reflectivity, and erythemal irradiance from sunrise to sunset for the whole earth as viewed by the DSCOVR spacecraft from the earth–sun Lagrange 1 orbit, 2017, Atmos. Meas. Tech., 10, 1–18, https://www.atmos-meas-tech.net/11/177/2018/

Ji, Q. and S.-C. Tsay (2000) On the dome effect of Eppley oyrgeometers and pyranometers, Geophys. Res. Lett.m 27:971-974, 2000.

Kazantzidis, A., Bais, A. F., Emde, C., Kazadzis, S., and Zerefos, C. S.: Attenuation of global ultraviolet and visible irradiance over Greece during the total solar eclipse of 29 March 2006, Atmos. Chem. Phys., 7, 5959-5969, https://doi.org/10.5194/acp-7-5959-2007, 2007.

Kopp, G.; Lean, J. L., (2011), A new, lower value of total solar irradiance: Evidence and climate significance, *Geophysical Research Letters*. 38, 2011.

483 Littmann, Mark; Espenak, Fred; Wilcox, Ken (2008). Totality: Eclipses of the Sun. Oxford University
484 Press. pp. 18–19. ISBN 0-19-953209-5. 2008.

485 Liendo, J.A. and G.H. Chacin, (2004), A study of a solar eclipse using a photocell, Revista Brasileira de
486 Ensino de Fisica, v. 26, 395 – 399, 2004.

487 Maignan, F., Breon, F. M., and Lacaze, R., (2004), Bidirectional reflectance of Earth targets: Evaluation of
488 analytical models using a large set of spaceborne measurements with emphasis on the Hot Spot,
489 Remote Sens. Environ., 90, 210–220, doi:10.1016/j.rse.2003.12.006, 2006

490 Marshak, A., J. Herman, A. Szabo, K. Blank, S. Carn, A. Cede, I. Geogdzhayev, D. Huang, L. Huang, Y.
491 Knyazikhin, M. Kowalewski, N. Krotkov, A. Lyapustin, R. McPeters, K. Meyer, O. Torres, and Y. Yang,
492 2018: Earth Observations from AMERICAN METEOROLOGICAL SOCIETY DSCOVR/EPIC Instrument. Bull.
493 Amer. Meteor. Soc. doi:10.1175/BAMS-D-17-0223.1, in press, 2018.
494 https://journals.ametsoc.org/doi/abs/10.1175/BAMS-D-17-0223.1
495

496 Mayer, B. and Kylling, (2005) A.: Technical Note: The libRadtran software package for radiative transfer
497 calculations: Description and examples of use, Atmos. Chem. Phys., 5, 1855–1877, http://www.atmos-
498 chem-phys.net/5/1855/2005/, 2005.
499

500 Meeus, J. (2003). "The maximum possible duration of a total solar eclipse". *Journal of the British*
501 *Astronomical Association*. **113** (6): 343–48.

502 Psiloglou, B.E. and H. D. Kambezidis, Performance of the meteorological radiation model during the solar
503 eclipse of 29 March 2006, Atmos. Chem. Phys., 7, 6047–6059, 2007.

504 Wen, G., A. Marshak, and R.F. Cahalan, (2008) Importance of molecular Rayleigh scattering in the
505 enhancement of clear sky radiance in the vicinity of boundary layer cumulus clouds. J. Geophys. Res.,
506 113: [10.1029/2008JD010592], 2008.

507

513

514 **Tables**

515

Table 1 *Eclipse Measurement Timing and Location Details for 5 Wavelengths*

Eclipse Maximum and EPIC Image Times. Total Measurement Duration 2.7 minutes

Wavelength (nm)	Date and Time	Location Name	Longitude
	2017-08-21 17:35:40	Eclipse West Edge of WY state	-111°02'
551	2017-08-21 17:42:36	West of Casper	-106°22'
680	2017-08-21 17:43:30	West of Casper	-106°21'
Casper Wyoming	2017-08-21 17:43:51	Casper WY	-106°19'
780	2017-08-21 17:44:24	Near Glenrock WY	-105°52'
443	2017-08-21 17:44:50	West of Douglas WY	-105°14'
388	2017-08-21 17:45:18	West of Douglas WY	-105°17'
	2017-08-21 17:48:04	Eclipse East Edge of WY state	-104°03'

516

517

518

Table 2 *Radiance Ratio $R_{EN}(\lambda_i)$ during eclipse totality 17:45 UTC compared to 20 Aug*

Wavelength λ_i (nm)	Max. $R_{EN}(\lambda_i)$ C/s
317.5	118
325	68.2
340	144
388	86
443	122
551	119.5
680	80
688	38
764	108
780	112.5

519

520

521

522

523

524

525

526

Table 3A Eclipse change in reflected light at Casper, WY from 20, 21, 23 August 2017 Units are ICs x 10^{-7}

λ_i (nm)	20 August 2017 16:58:31 GMT	21 August 2017 17:44:50	23 August 2017 17:54:36	Avg. PDF
317.5	280.5	258.8	282.0	9±0.3
325	460.6	425.5	464.2	9±0.4
340	3183	2946	3213	9±0.5
388	2034	1878	2044	9±0.3
443	5808	5344	5813.2	9±0.05
551	5619	5078	5573	10±0.5
680	3790	3433	3773	10±0.3
688	1129	1010	1110	11±0.9
764	671.9	585.9	651.9	13±1.7
780	2794	2491	2799	12±0.1

527

Table 3B Eclipse change in reflected light at Columbia, MO from 20, 21, 23 August 2017 Units are ICs x 10^{-7}

λ_i (nm)	20 August 2017 18:03:359 GMT	21 August 2017 18:14:50	23 August 2017 17:54:36	Avg. PDF
317.5	281.3	258.3	282.0	9±0.1
325	461.6	425.9	464.2	9±0.3
340	3193	2956	3213	8±0.3
388	2034	1884	2044	8±0.3
443	5813.7	5372.3	5813.2	8±0.01
551	5586	5091	5573	10±0.1
680	3790	3453	3773	10±0.2
688	1121	1011	1110	10±0.5
764	661.2	576.0	651.9	14±0.8
780	2794	2475	2799	13±0.1

528

529

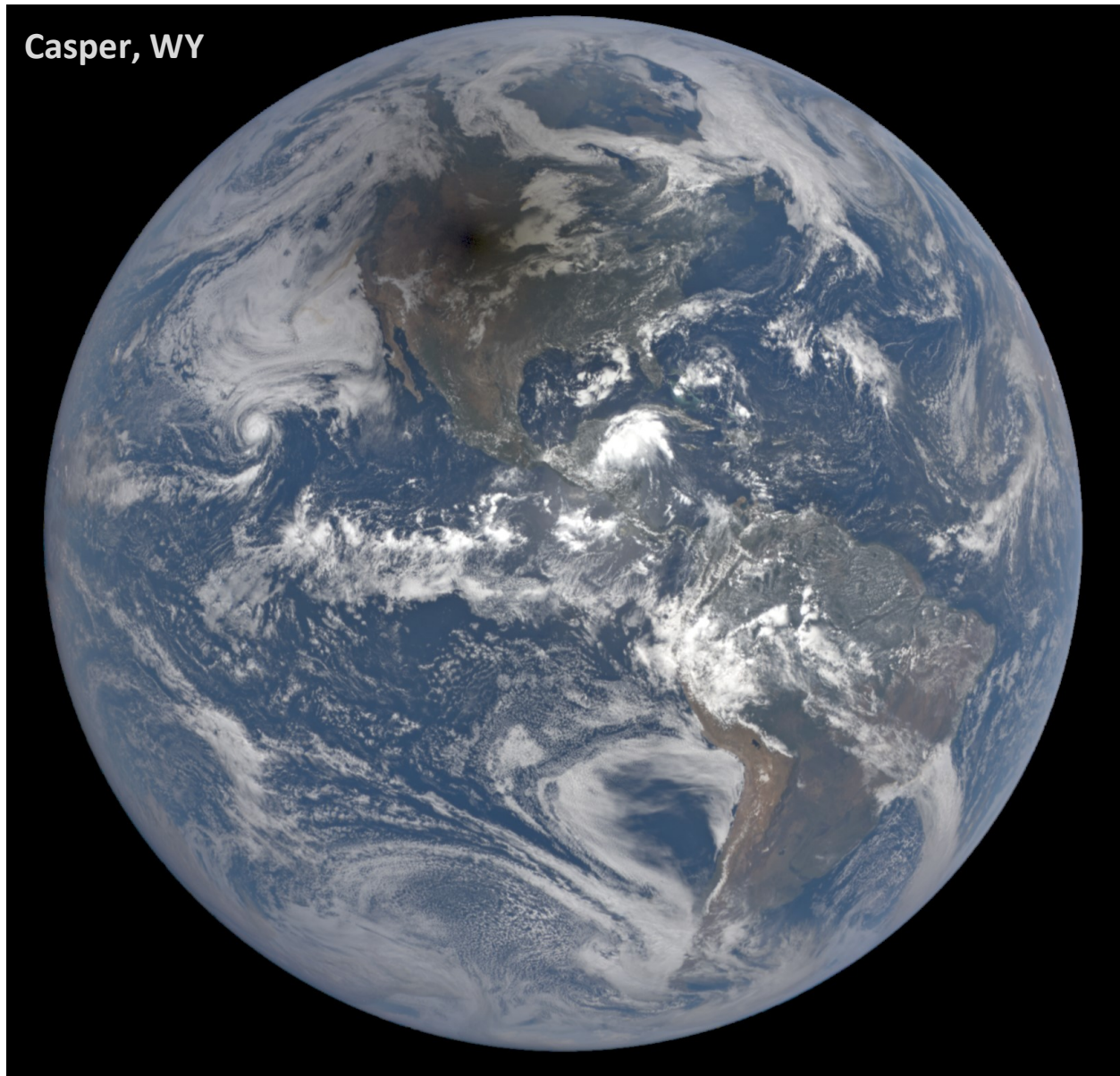530

531

Figure Captions

533   Fig. 1 Synoptic view of the sunlit Earth perturbed by the 21 August 2017 total eclipse centered over
534   Casper, Wyoming at 17:44:50 UTC. The black region is the eclipse umbra centered over Casper, WY. The
535   color image has been adjusted from the images on https://epic.gsfc.nasa.gov/ by increasing the gamma
536   correction (Cescatti, 2007) to bring out the region of totality and surrounding clouds.

537   Fig. 2 Synoptic view of the total eclipse centered over Columbia, Missouri at 18:14:50 UTC. The black
538   region is the eclipse umbra centered over Columbia, MO. The color image has been adjusted from the
539   images on https://epic.gsfc.nasa.gov/ by increasing the gamma correction to bring out the region of
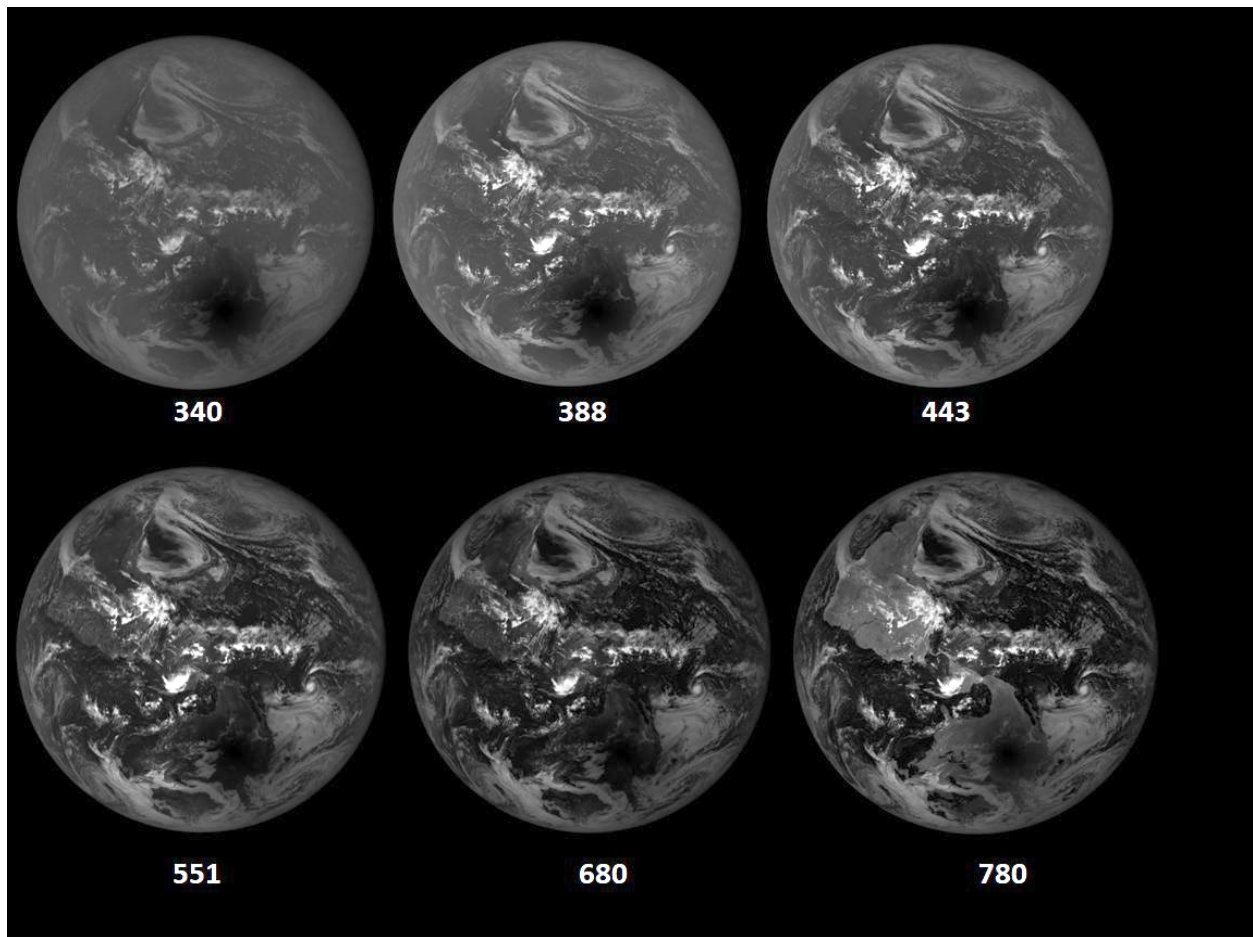540   totality and surrounding clouds.

541   Fig. 3 Greyscale images for 6 of the DSCOVR/EPIC channels for the eclipse over Casper Wyoming
542   showing the blurring caused by Rayleigh scattering and the dark land and ocean surfaces at 340 nm to
543   the almost clear atmosphere and bright continental surfaces at 780 nm. The images were obtained over
544   a period of 2.7 minutes. North is facing down. The greyscale is linear, with black representing very low
545   reflectivity and white very high reflectivity from high altitude equatorial region clouds.
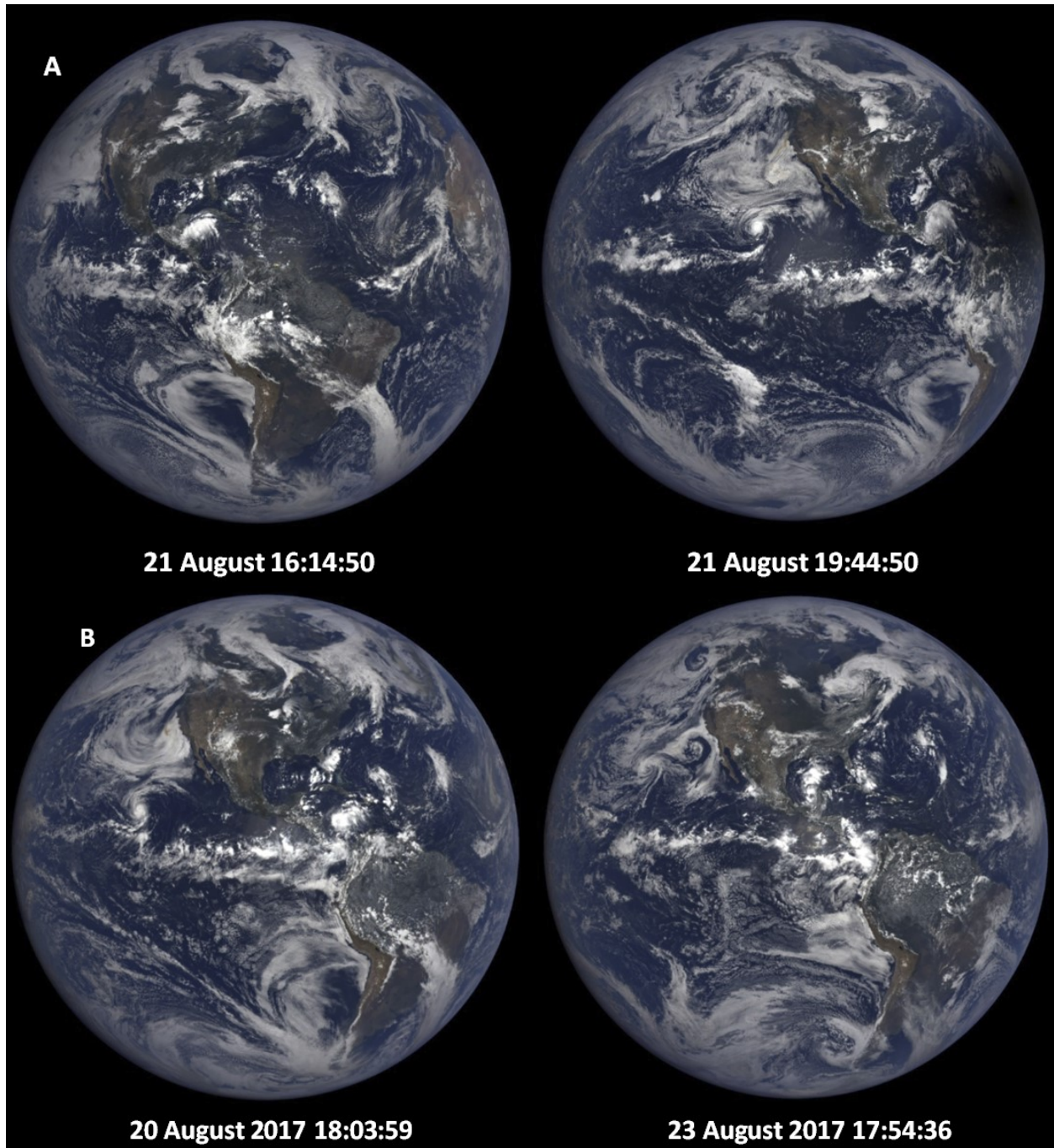
546   Fig. 4 Panel A: Synoptic natural color images on 21 August at 16:14 and 19:44 before and after the
547   eclipse over the US, and Panel B: the days before and after the eclipse selected to be as close as possible
548   to the phase angle (UTC 17:44:50) as the time of totality over Casper, Wyoming. North is facing up.

549   Fig. 5 Top: The effect of an eclipse (21 Aug) on the measured C/s reflected back to space as a function of
550   longitude (degrees) for two locations, Casper Wyoming (left) and Columbia Missouri (right). Bottom:
551   Measured C/s reflected back to space on 20 Aug. A $\log_{10}$ scale is used to show details of the spatial
552   variability mostly caused by clouds

553   Fig. 6a   The ratio $R_{EN}(\lambda_i)$ = I(Aug20)/I(Aug21) at the time of the Eclipse in Casper Wyoming for
554   wavelengths 317.5 to 780 nm. The channels 317.5 to 340 nm are affected by ozone absorption and the
555   channels 688 and 764 nm are within the O_2 B and A absorption bands.

556   Fig. 6b The ratio $R_{EN}(\lambda_i)$ = I(Aug20)/I(Aug21) at the time of the Eclipse in Columbia, Missouri for
557   wavelengths 317.5 to 780 nm. The channels 317.5 to 340 nm are affected by ozone absorption and the
558   channels 688 and 764 nm are within the O_2 B and A absorption bands.

559   Fig. 7 The C/s observed by EPIC for the 443 nm channel corresponding to the color image shown in Fig.
560   1. In the data file, the word infinity has been replaced by the number zero. In this image there are
561   approximately Np = 2.59×10^6 illuminated pixels out of 2048^2 = 4.194304×10^6 pixels (61.8 %).

562   Fig. 8a Image in C/s for 340 and 388 nm for 20 Aug.(A+D), 21 Aug. (B+E), and 23 Aug. (C+F). The scale
563   applies to the specific wavelength. North is up.

564   Fig. 8b Image in C/s for 443 and 551 nm for 20 Aug.(A+D), 21 Aug. (B+E), and 23 Aug. (C+F). The scale
565   applies to the specific wavelength. North is up.

566   Fig. 8c Image in C/s for 680 and 780 nm for 20 Aug.(A+D), 21 Aug. (B+E), and 23 Aug. (C+F). The scale
567   applies to the specific wavelength. North is up.

568   Fig. 9 Average reflected light in C/s for eclipse (21 Aug. red) and non-eclipse (20 Aug. and 23 Aug. (black
569   and grey) days from Table 3 and Eqn. 1 for Casper and Columbia. The locations of the maxima are from
570   curve fitting to the discrete wavelength measurements.

571   Fig. 10 Solar Irradiance at 1 AU F(λ) Watts/(m^2 nm) (Mayer and Kylling, 2005) and the eclipse reduction
572   function R(λ) in percent for Casper, Wyoming (red curve in panel A) and Columbia, Missouri (red curve
573   in panel B). Fractional reduction (nm^{-1}) in reflected solar irradiance in the direction of L-1 for Casper,
574   Wyoming (panel C) and Columbia, Missouri (panel D)

575   Fig. 11 A. The measured albedo at Casper Wyoming on 20 Aug (black curve) and 23 Aug (grey curve)
576   compared to B the POLDER measured surface reflectance in the Khingan Range, China (Maignan et al.,
577   2004) corresponding to 8$^{\text{o}}$ from overhead sun.

578   Fig. A1 The timing and shape of the Moon's shadow over Casper, Wyoming showing the relative location
579   of Casper and Columbia (white circles) at 11:45 MDT (Mountain Daylight Time) and 1:15 CDT (Central
580   Daylight Time). The shadow is moving at about 46 km/minute. ([https://eclipse2017.nasa.gov/eclipse-](https://eclipse2017.nasa.gov/eclipse-maps)
581   [maps](https://eclipse2017.nasa.gov/eclipse-maps)). The scale size with the NASA logo is 50 km.

582   Fig. A2a Image in C/s for 317 and 340 nm for 20 Aug., 21 Aug. and 23 Aug. The scale applies to the
583   specific wavelength. North is up.

584   Fig. A2b Image in C/s for 340 and 388 nm for 20 Aug.(A+C), 21 Aug. (B+E), and 23 Aug. (C+F). The scale
585   applies to the specific wavelength. North is up.

586   Fig. A2c A2c Image in C/s for 688 and 764 nm for 20 Aug., 21 Aug. and 23 Aug. The scale applies to the
587   specific wavelength. North is up.

588   Fig. A3 EPIC measured ozone amounts from 20 August in the vicinity of Casper, WY and Columbia, MO.

589

Fig. 1 Synoptic view of the sunlit Earth perturbed by the 21 August 2017 total eclipse centered over Casper, Wyoming at 17:44:50 UTC. The black region is the eclipse umbra centered over Casper, WY. The color image has been adjusted from the images on https://epic.gsfc.nasa.gov/ by increasing the gamma correction (Cescatti, 2007) to bring out the region of totality and surrounding clouds.

590

591

F01

593

Columbia, MO

Fig. 2 Synoptic view of the total eclipse centered over Columbia, Missouri at 18:14:50 UTC. The black region is the eclipse umbra centered over Columbia, MO. The color image has been adjusted from the images on https://epic.gsfc.nasa.gov/ by increasing the gamma correction to bring out the region of totality and surrounding clouds.

594

595

596 **F02**

597

Greyscale images for 6 of the DSCOVR/EPIC channels for the eclipse over Casper Wyoming showing the blurring caused by Rayleigh scattering and the dark land and ocean surfaces at 340 nm to the almost clear atmosphere and bright continental surfaces at 780 nm. The images were obtained over a period of 2.7 minutes. North is facing down. The greyscale is linear, with black representing very low reflectivity and white very high reflectivity from high altitude equatorial region clouds.

F03

Fig. 4 Panel A: Synoptic natural color images on 21 August at 16:14 and 19:44 before and after the eclipse over the US, and Panel B: the days before and after the eclipse selected to be as close as possible to the phase angle (UTC 17:44:50) as the time of totality over Casper, Wyoming. North is facing up.

604

605   **F04**

606
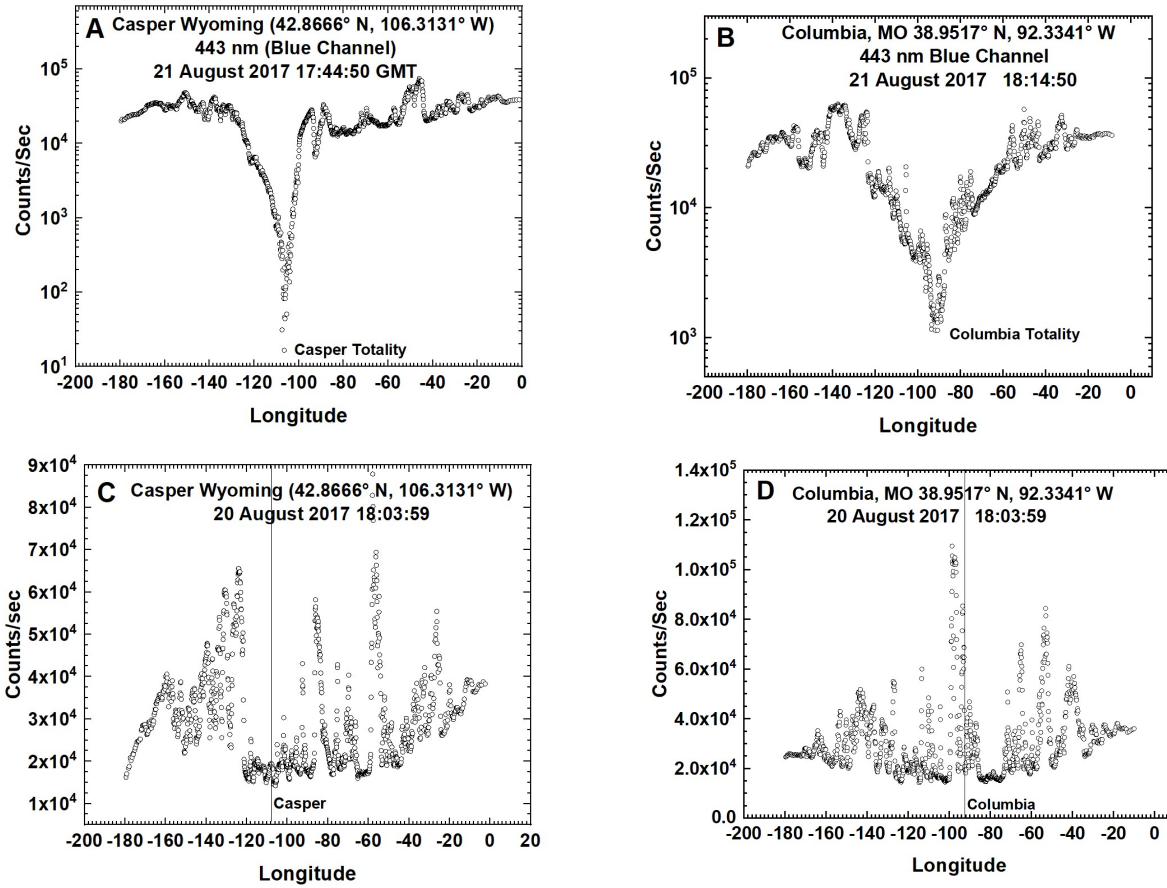
Fig. 5 Top: The effect of an eclipse (21 Aug) on the measured C/s reflected back to space as a function of longitude (degrees) for two locations, Casper Wyoming (left) and Columbia Missouri (right). Middle: Measured C/s reflected back to space on 20 Aug.

607

608

609 **F05**

610

611
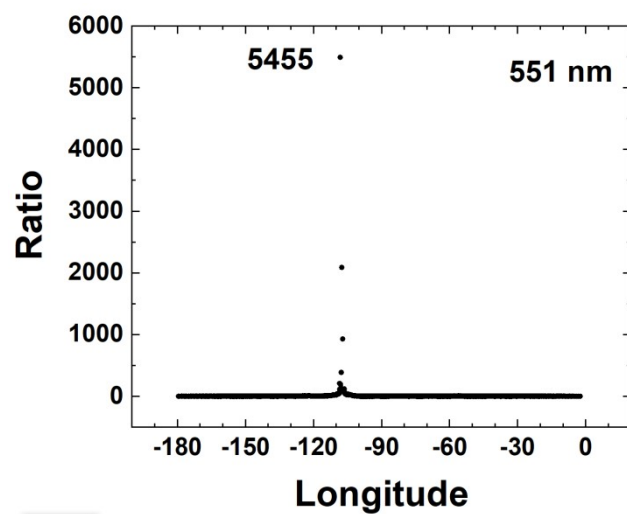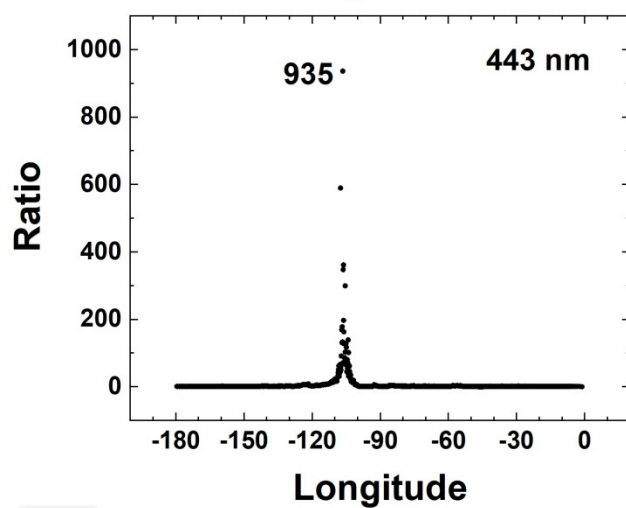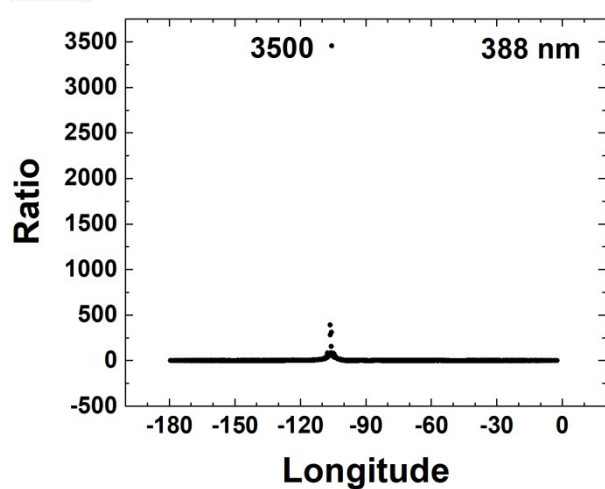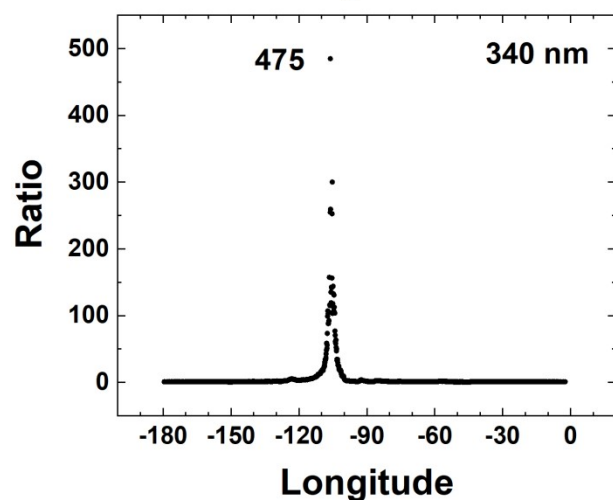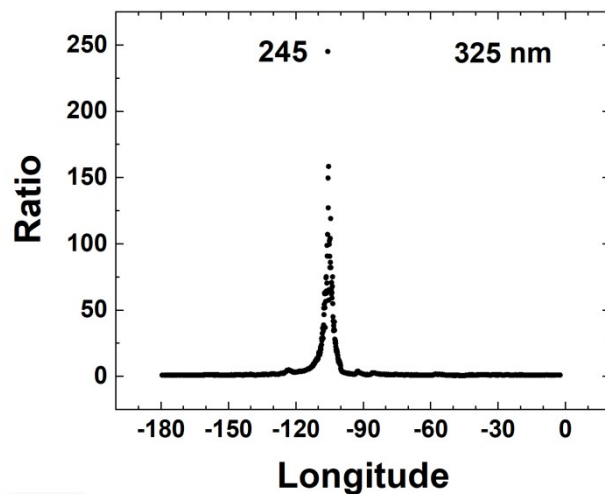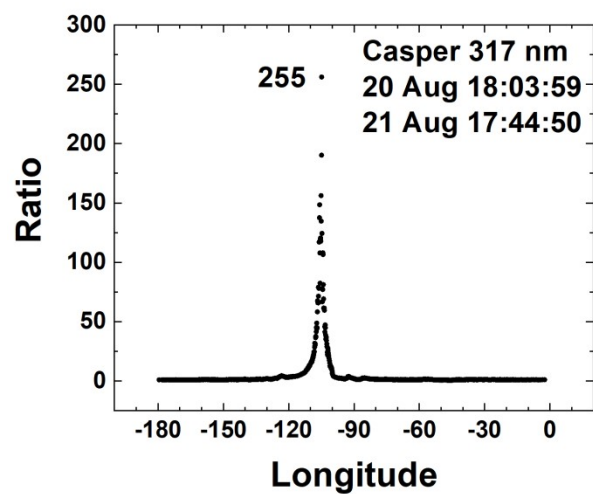
F06a
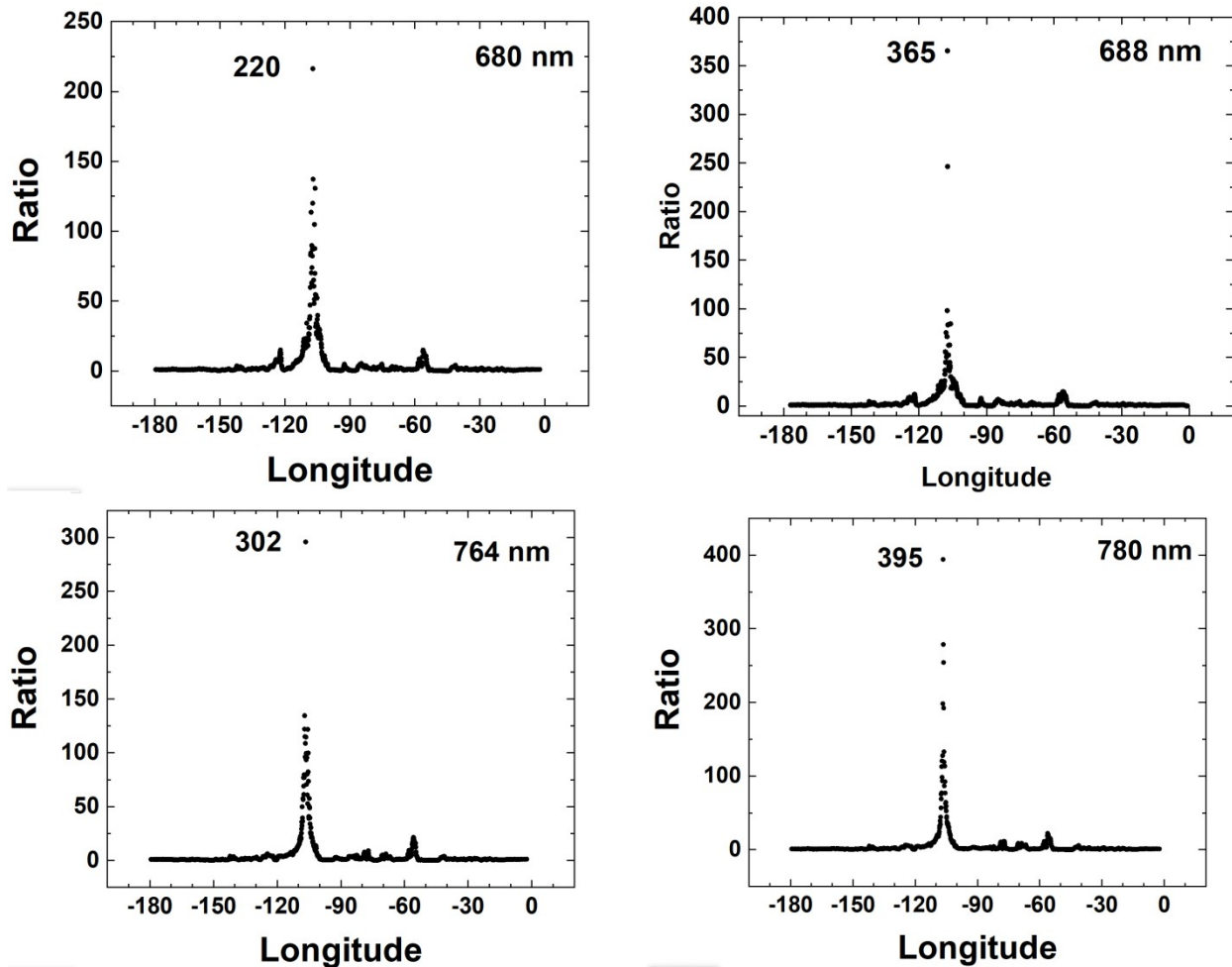
Fig. 6a. The ratio $R_{EN}(\lambda_i)$ = I(Aug20)/I(Aug21) at the time of the Eclipse in Casper Wyoming for wavelengths 317.5 to 780 nm. The channels 317.5 to 340 nm are affected by ozone absorption and the channels 688 and 764 nm are within the O_2 B and A absorption bands.

613

614

615 **F06a Continued**
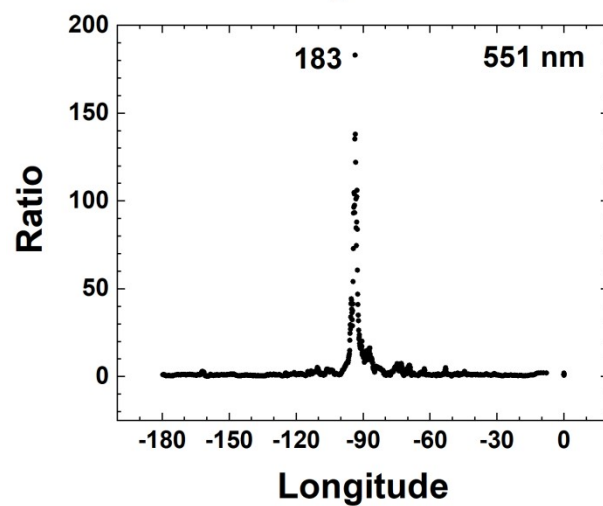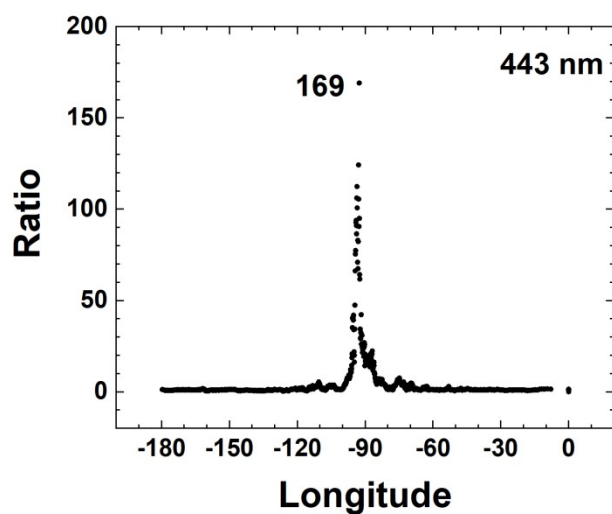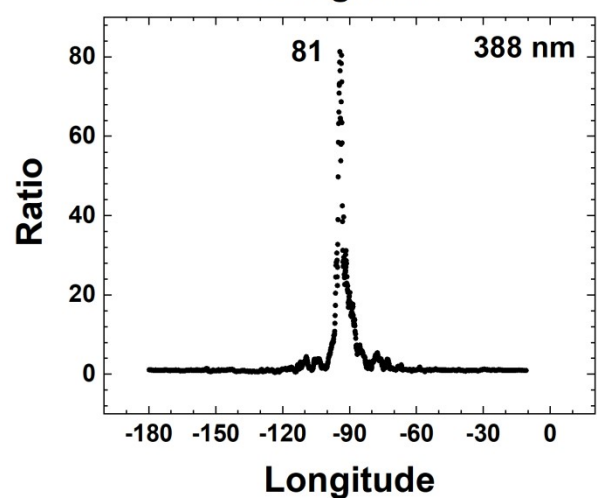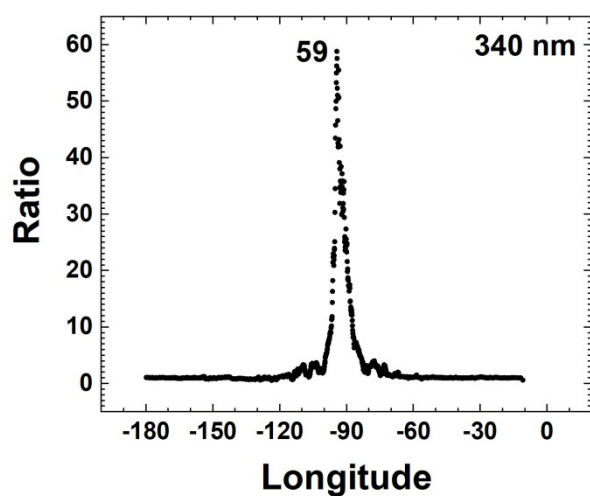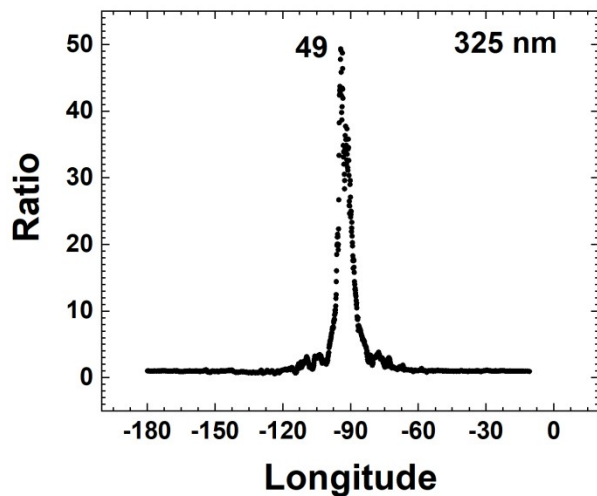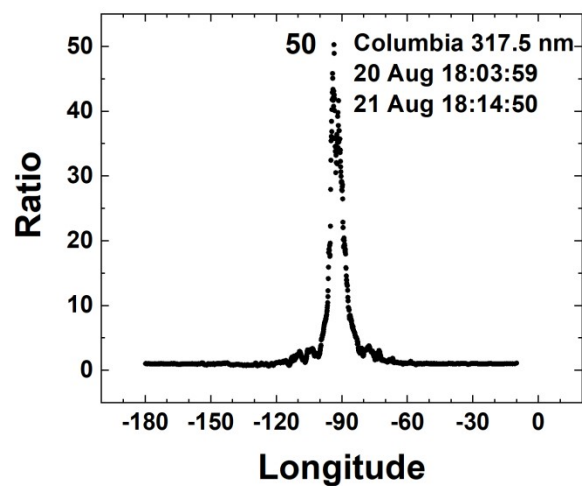
F06b
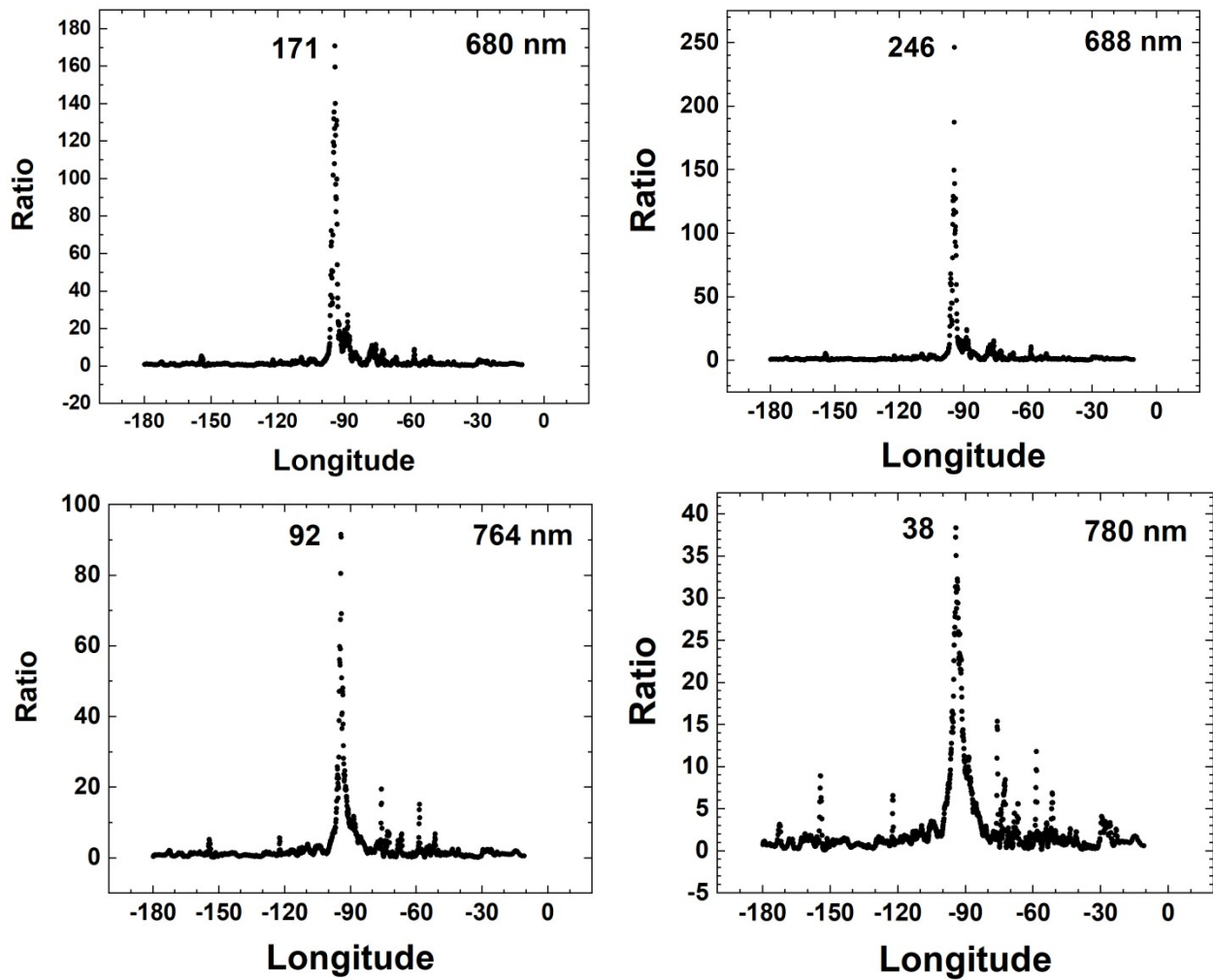
Fig. 6b. The ratio $R_{EN}(\lambda_i)$ = I(Aug20)/I(Aug21) at the time of the Eclipse in Columbia, Missouri for wavelengths 317.5 to 780 nm. The channels 317.5 to 340 nm are affected by ozone absorption and the channels 688 and 764 nm are within the O_2 B and A absorption bands.

618

619

620

F06b Continued

622

623
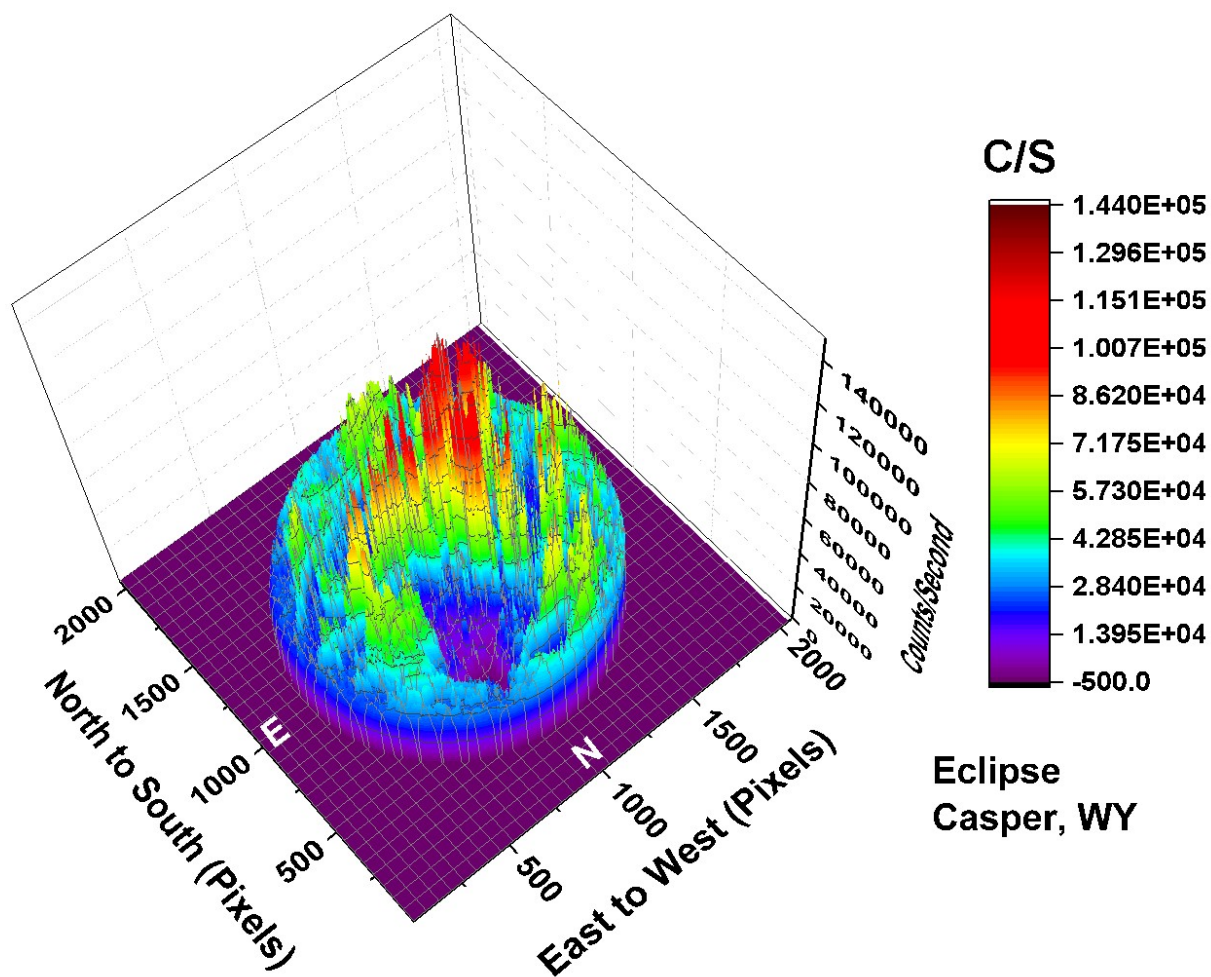
Fig. 7 The C/s observed by EPIC for the 443 nm channel corresponding to the color image shown in Fig. 1. In the data file, the word infinity has been replaced by the number zero. In this image there are approximately 2.59×10^6 illuminated pixels out of $2048^2 = 4.194304 \times 10^6$ pixels (61.8 %).

624

625

626   **F07**

627
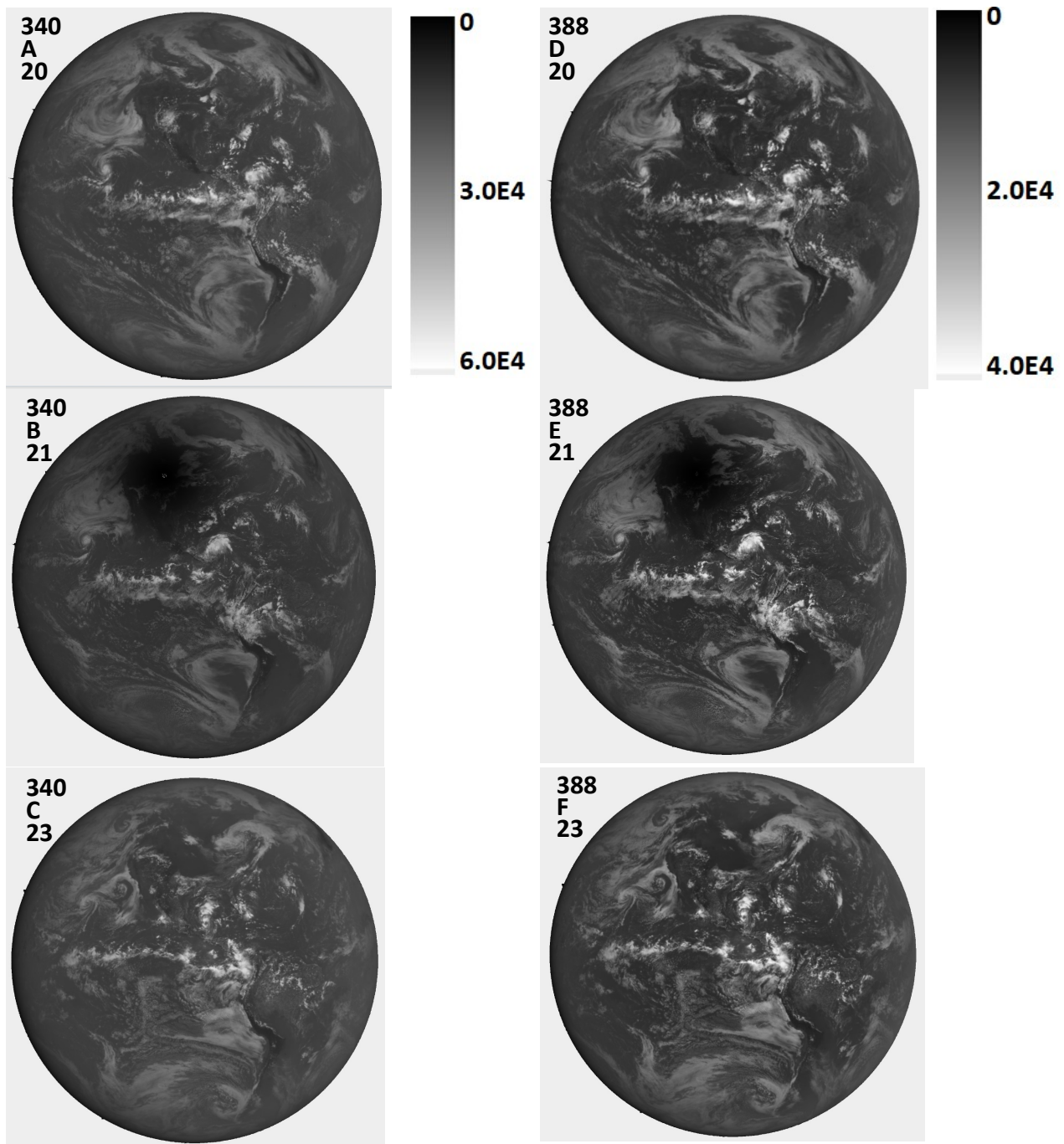
Figure 8a Image in C/s for 340 and 388 nm for 20 Aug.(A+D), 21 Aug. (B+E), and 23 Aug. (C+F). The scale applies to the specific wavelength. North is up.

628

F08a
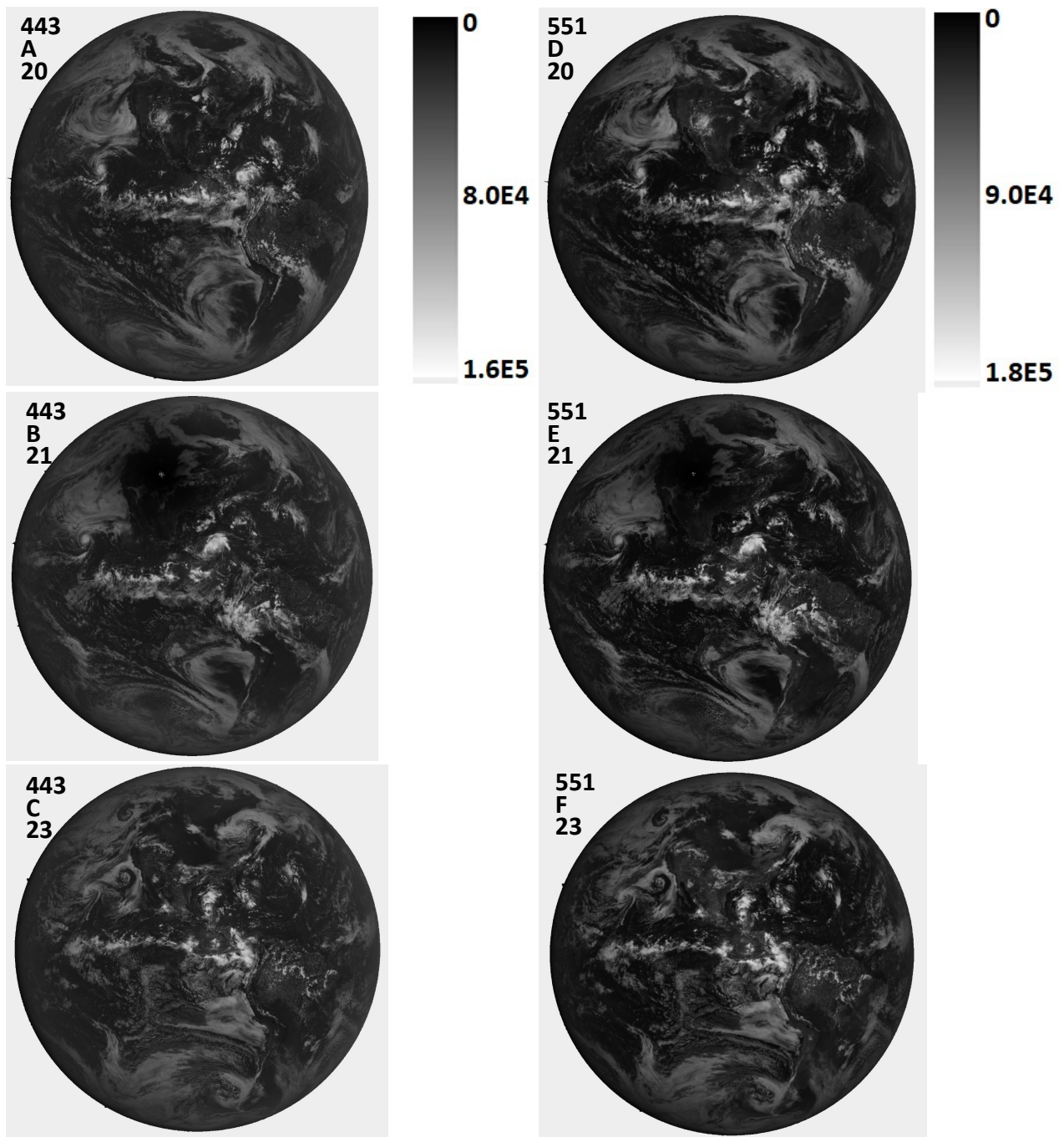
Figure 8b Image in C/s for 443 and 551 nm for 20 Aug.(A+D), 21 Aug. (B+E), and 23 Aug. (C+F). The scale applies to the specific wavelength. North is up.

629

630

631 **F08b**
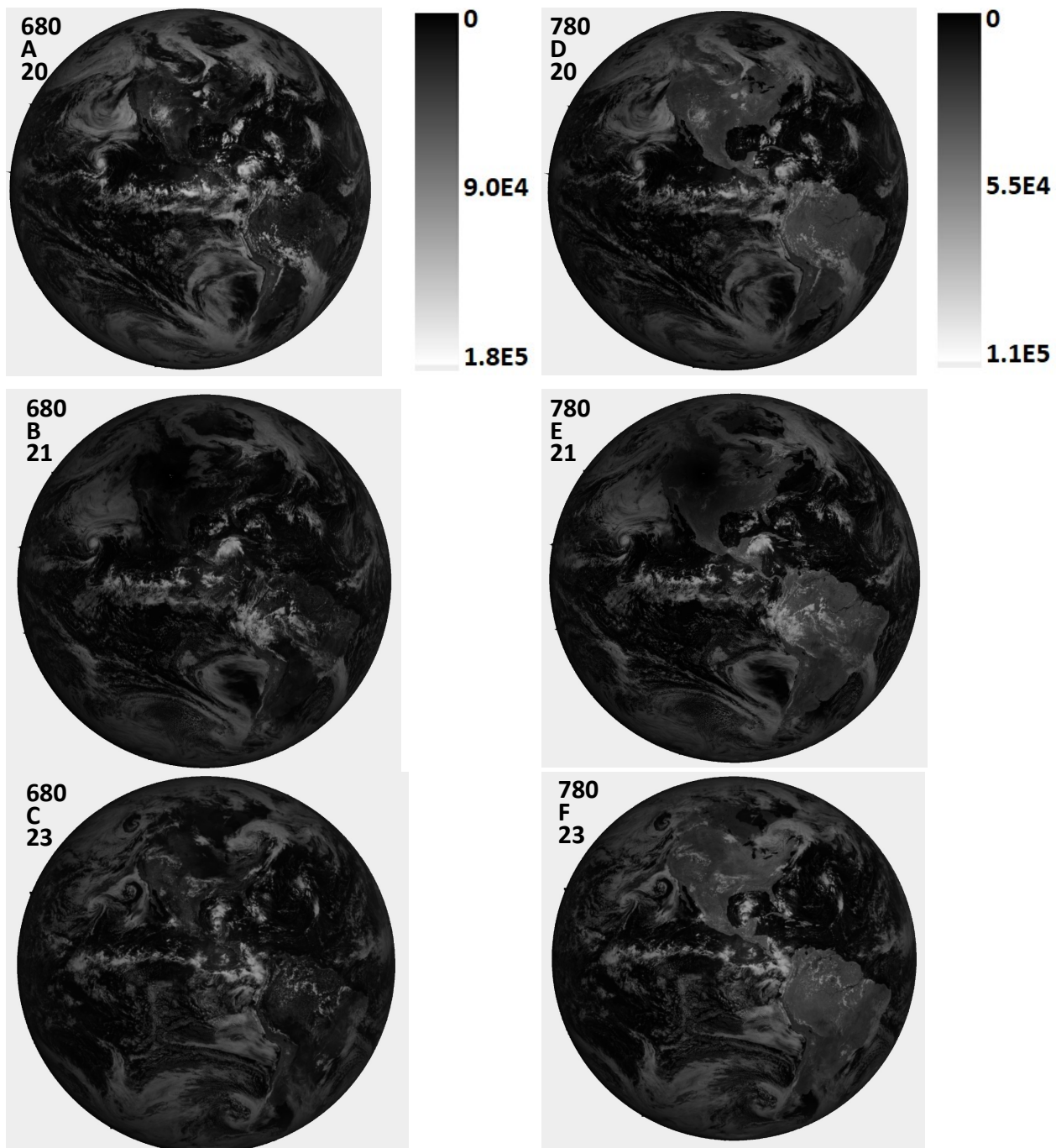
Figure 8c Image in C/s for 680 and 780 nm for 20 Aug.(A+D), 21 Aug. (B+E), and 23 Aug. (C+F). The scale applies to the specific wavelength. North is up.

632

633

634 **F08c**

635
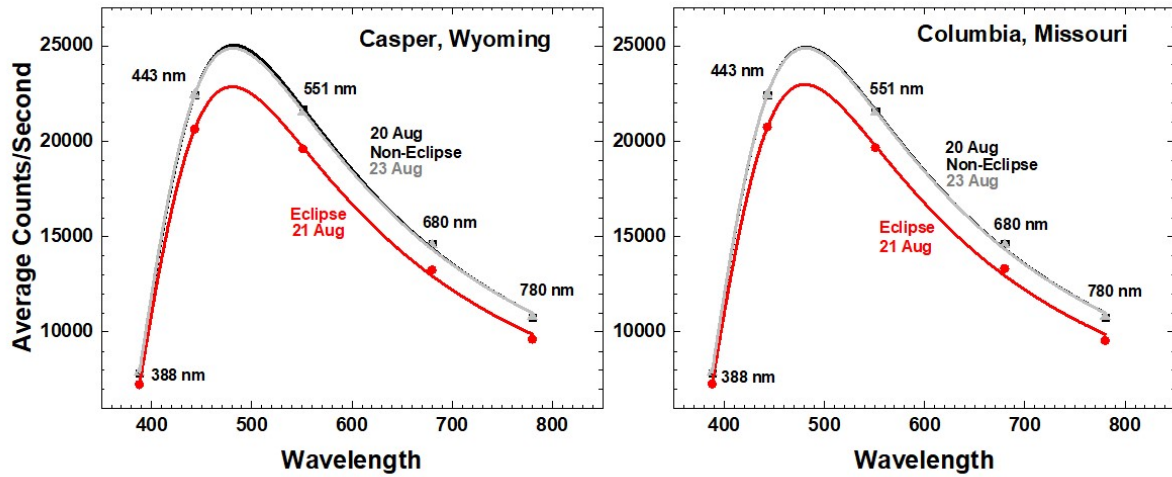
Fig. 9 Average reflected light in C/s for eclipse (21 Aug. red) and non-eclipse (20 Aug. and 23 Aug. (black and grey) days from Table 3 and Eqn. 1 for Casper and Columbia. The locations of the maxima are from curve fitting to the discrete wavelength measurements.
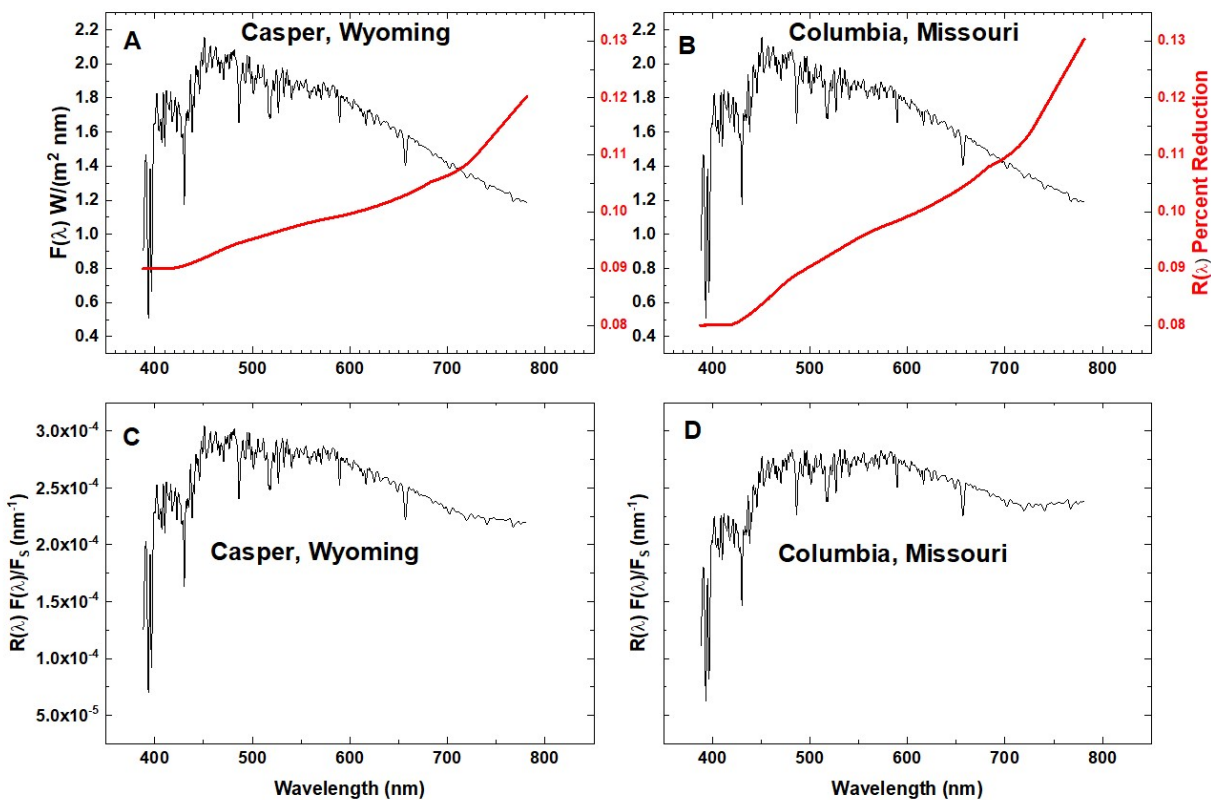
636

637

638   **F09**

639

640

Fig. 10 Solar Irradiance at 1 AU F(λ) Watts/(m^2 nm) (Mayer and Kylling, 2005) and the eclipse reduction function R(λ) in percent for Casper, Wyoming (red curve in panel A) and Columbia, Missouri (red curve in panel B). Fractional reduction (nm^{-1}) in reflected solar irradiance in the direction of L-1 for Casper, Wyoming (panel C) and Columbia, Missouri (panel D)
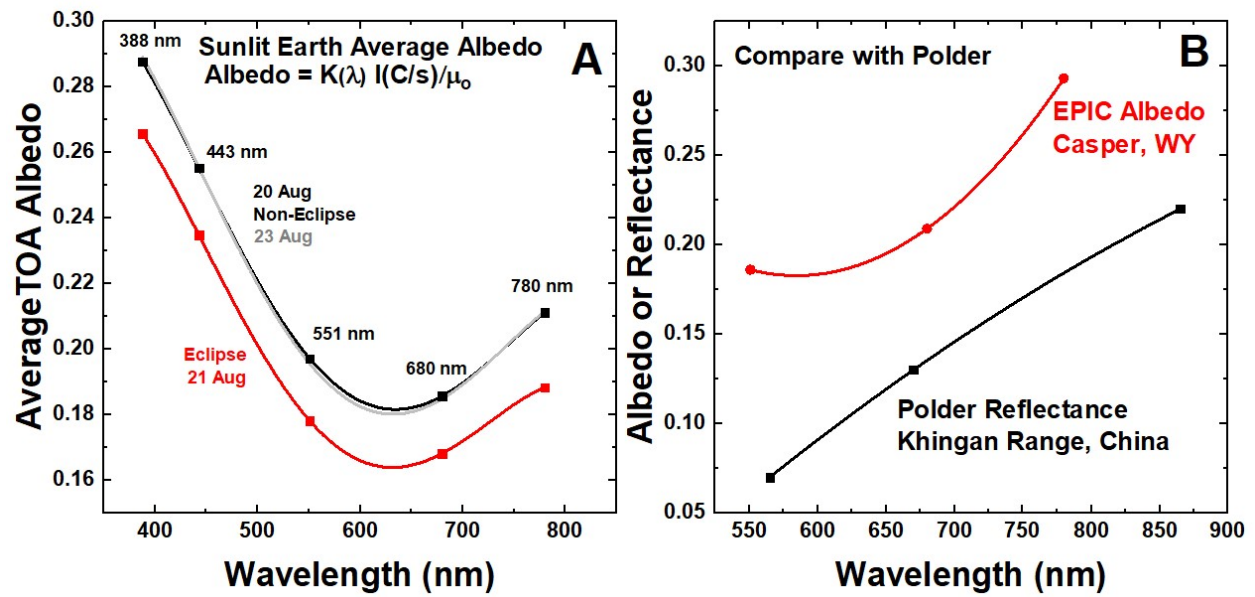
641

642

643

F10

645

Fig. 11 A. The measured albedo at Casper Wyoming on 20 Aug (black curve) and 23 Aug (grey curve) compared to B the POLDER measured surface reflectance in the Khingan Range, China (Maignan et al., 2004) corresponding to 8° from overhead sun.
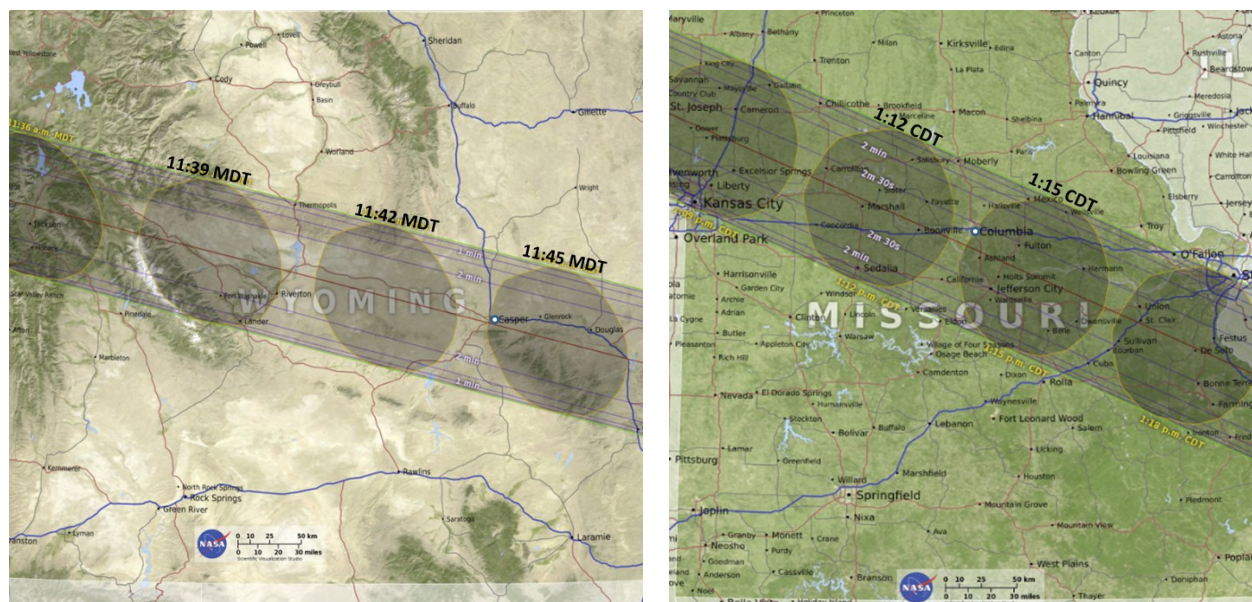
646

647 **F11**

648

Fig. A1 The timing and shape of the Moon's shadow over Casper, Wyoming showing the relative location of Casper and Columbia (white circles) at 11:45 MDT (Mountain Daylight Time) and 1:15 CDT (Central Daylight Time). The shadow is moving at about 46 km/minute. (https://eclipse2017.nasa.gov/eclipse-maps). The scale size with the NASA logo is 50 km.

651
652

653   **FA1**
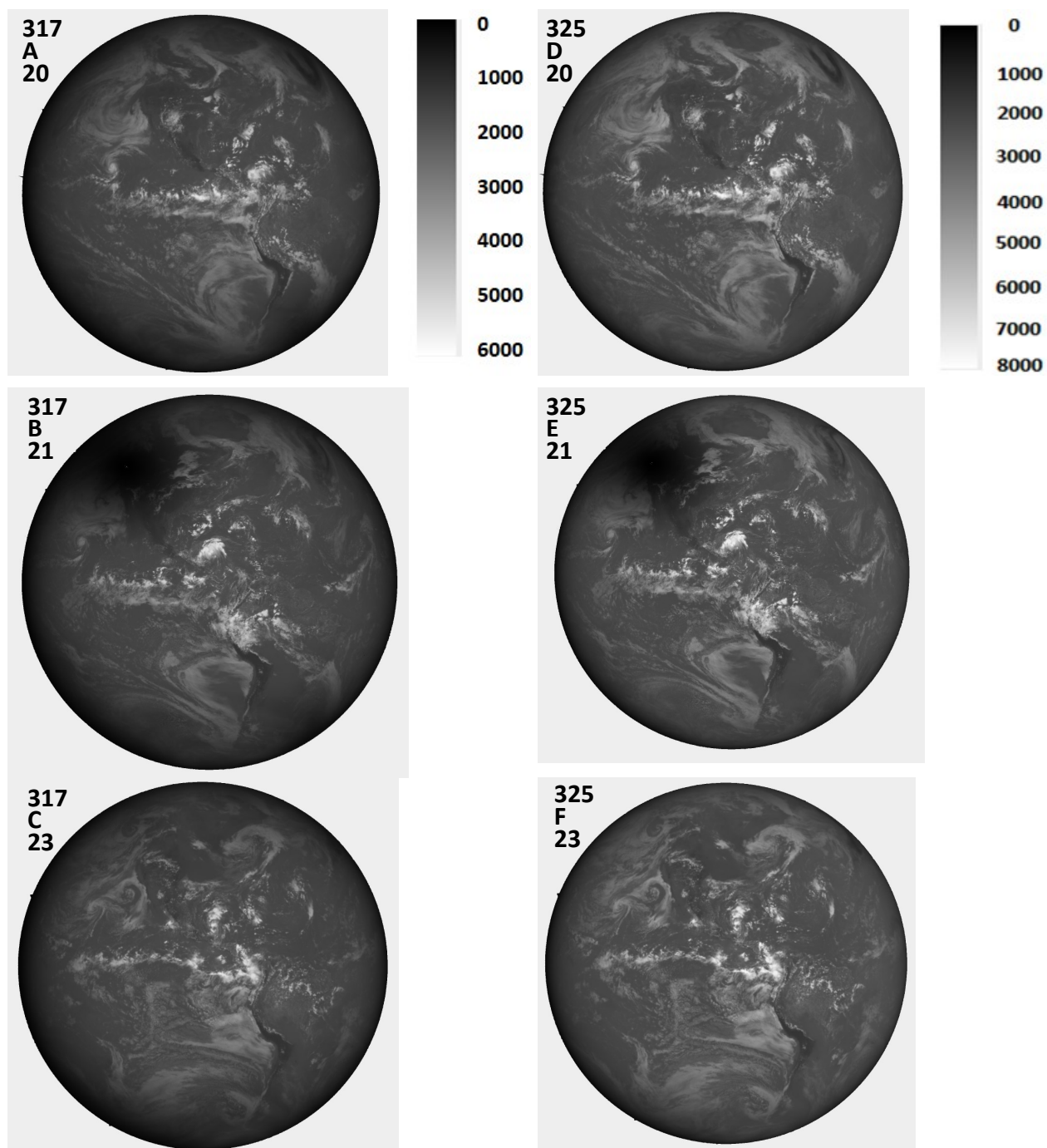
Fig. A2a Image in C/s for 317 and 340 nm for 20 Aug., 21 Aug. and 23 Aug. The scale applies to the specific wavelength. North is up.

FA2

688 A 20
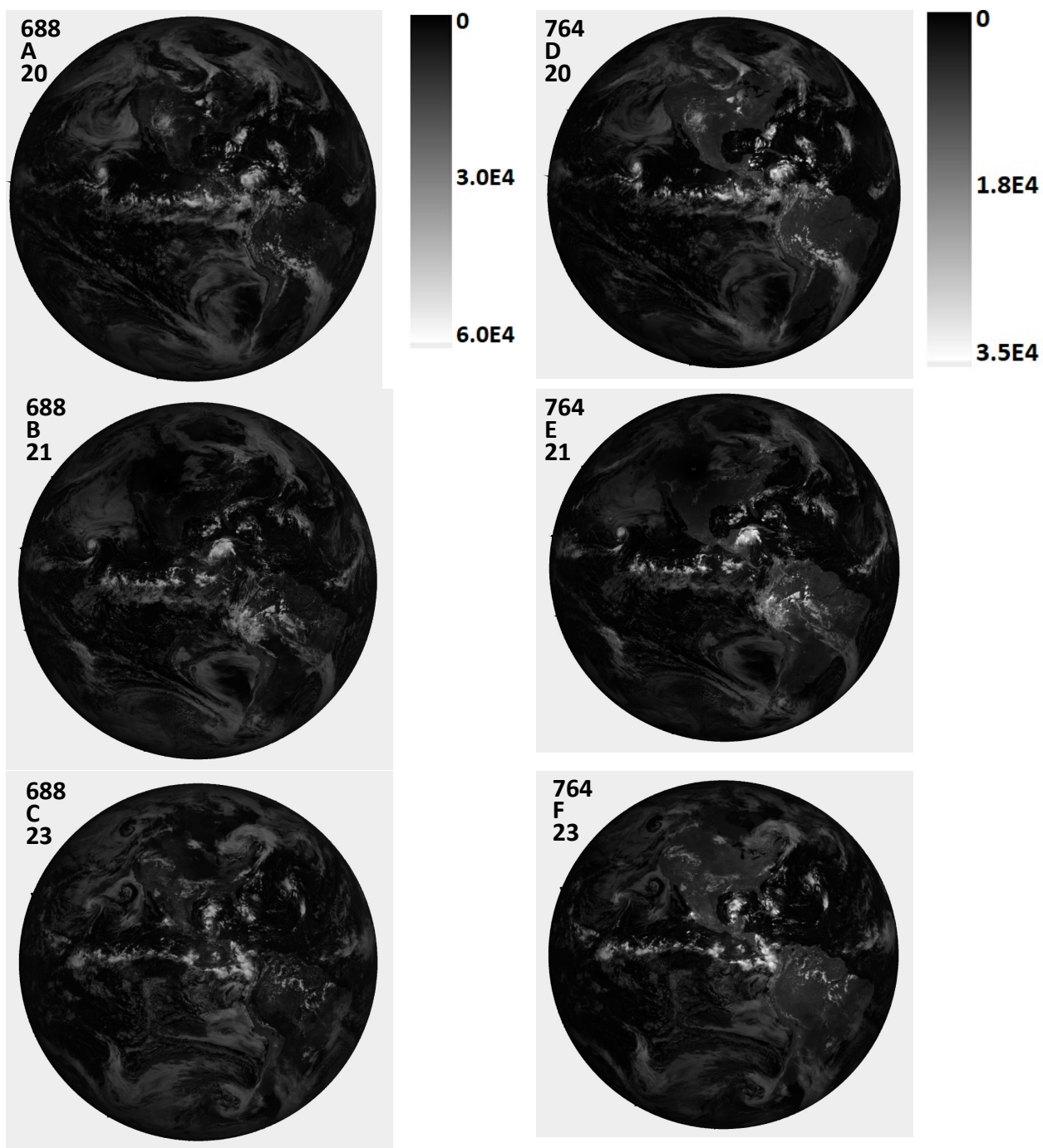
0

3.0E4

6.0E4

764 D 20

0

1.8E4

3.5E4

688 B 21

764 E 21

688 C 23

764 F 23

Fig. A2b Image in C/s for 688 and 764 nm for 20 Aug., 21 Aug. and 23 Aug. The scale applies to the specific wavelength. North is up.

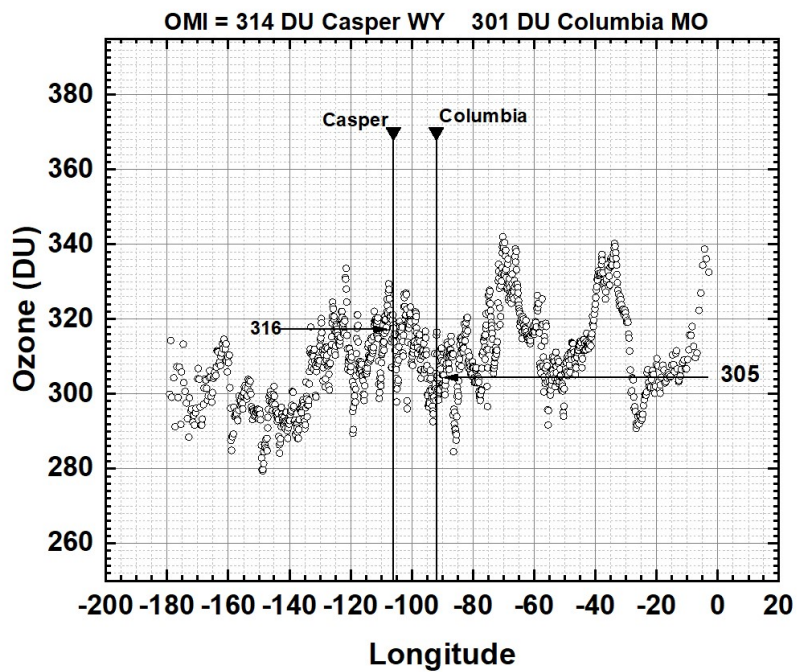**OMI = 314 DU Casper WY   301 DU Columbia MO**

Fig. A3 EPIC measured ozone amounts from 20 August in the vicinity of Casper, WY and Columbia, MO.

660

661

662

663 **FA3**